Study of the pyrolysis reaction mechanisms for dust explosion

Peter Badu

IMT Mines Albi-Carmaux
École Mines-Télécom

LABORATOIRE REACTIONS ET GENIE DES PROCEDES, CNRS, UMR 7274

MASTER THESIS

Presented and defended on:

15th September, 2021

In Partial Fufillment of the Requirement for the Degree of Master of Science

In Biomass and Waste for Energy and Materials

By

Peter Opoku BADU

STUDY OF THE PYROLYSIS REACTION MECHANISMS FOR DUST EXPLOSION

JURY COMPOSITION

Company Tutors:	Prof. Olivier DUFAUD	University of Lorraine
	Mr. Matteo PIETRACCINI	University of Lorraine
School Tutor:	Prof. Sylvian SALVADOR	IMT Mines Albi
	Prof. Patricia ARLABOSE	IMT Mines Albi
	Dr. Doan Pham MINH	IT Mines Albi

UNIVERSITÉ DE LORRAINE ENSIC LRGP LABORATOIRE RÉACTIONS ET GÉNIE DES PROCÉDÉS cnrs

ACKNOWLEDGEMENT

To begin with, I express my heartfelt and profound gratitude to Professor Olivier DUFAUD and Mr Matteo PIETRACCINI both my company tutors at Laboratoire Réactions et Génie des Procédés (LRGP), for welcoming and accepting me in their research team. Your unsurpassed team spirit, patience, cooperation and guidance during these past five months even under unprecedented stressful working conditions due to the COVID-19 pandemic made me enjoy working in this coveted research group. I offer my sincere appreciation for allowing me to learn, improve on my research skills and expand my academic network. Thank you!

A second thanks go to the lab technicians and Mr Yann LE BRECH, senior lecturer, Greener, whose advice and effort in the areas of instruments calibration made working in the laboratory smooth and less daunting. I appreciate the workshop team's efforts in making their machinery available for auxiliary instrumentation repairs and constructions required for successful experimental executions.

I would like to thank Centre National de la Recherché Scientifique (CNRS) for funding this research work as part of process safety for the environment.

I wish to acknowledge Professor Sylvian SALVADOR, a full-time professor at IMT MINES ALBI with much appreciation for having accepted to be my school tutor. Your constructive criticisms, remarks and unflinching interest was helpful in the completion of this work.

Special thanks go to Professor Patricia ARLABOSSE, head of the BIWEM master program and Lydie MIGNANO, head of international relations at IMT MINES ALBI for their unwavering support. Your presence has always been a source of encouragement during my master's formation. You offered a listening ear in crucial moments and were available for short and lengthier discussions when they were needed. The successful completion of the program could not have been done without your support, which cannot go unnoticed.

I owe my sincere thanks to my mum Comfort Christian and colleagues Ibrahim Isaah, Paul Iwunze, Vincent Dickson and Augustine Appiah Sekyi who have been behind the scenes and contributed indirectly to drive this work forward. Their inputs and support have been enormous and I am forever grateful for having known them.

I must express my gratitude to the members of my dissertation committee for painstakingly working with me on this project. Thank you for your extensive professional and scientific guidance in the realisation of this work.

Finally, I thank God for making everything happen.

CONTENTS

LIST OF TABLES

LIST OF FIGURES

RESEARCH CENTER AND RESEARCH GROUP PRESENTATION

I had the privilege to undertake my master thesis in partial fulfilment of the requirement for the degree of Master of Science in Biomass and Waste for Energy and Materials at Laboratoire Réaction et Génie des Procédés (LRGP)-ENSIC. Based in Nancy, LRGP (UMR 7274) is a Reaction and Process Engineering Laboratory formed from the consolidation of four different research units; the Laboratory of Chemical Engineering Sciences (LSGC), the Department of Physical Chemistry of Reactions (DCPR), The Laboratory of Thermodynamics of Polyphase Media (LTMP), and The Centre for Chemical Engineering of Rheologically Complex Media (GEMICO). The merger was completed on January 1, 2010, with the newly formed LRGP being a joint unit of CNRS and the University of Lorraine. LRGP is present over four sites with an overall land size of 9000m^2; (i) the National School of Chemical Industries (ENSIC-the main site), (ii) École Nationale Supérieure d'Agronomie et des Industries Alimentaires (ENSAIA), Vie et Santé (SVS) analytical platform at Nancy-Brabois plateau, and Bouzule farm site located in Champenoux.

LRGP's general objective is to develop the scientific and technological knowledge and expertise required for the design, study, management, and optimisation of complex physicochemical, and biological processes of matter transforms into energy. It currently employs over 300 people, consisting of CNRS researchers (20), research professors (80), technical and administrative staff (45) and 180 non-permanent staff. The laboratory's research teams are structured into five major axes illustrated in Figure 1.

Figure 1: LRGP-ENSIC SITE (1 Rue Grandville, Nancy to the left) and the research axes.

This research was conducted in the PErSeVAL axis.

Process for the Environment, Safety and Resource Recovery — (PErSeVAL) Axis

The PErSeVAL axis headed by Prof. Olivier Dufaud is sub-divided into the (i) Aerosol filtration and Safety Explosion (ii) Soil and Water, and (iii) Polyphase Systems research group.

The overall objectives of the PErSeVAL Axis involve:

a) use of multi-scale approaches to offer cleaner and safer processes.

b) development of innovative soil pollution, and effluent (liquid, gases, aerosols) treatment processes
c) development of environmental analysis tools for environmental impact and risks assessment
d) use of electrochemical processes for energy conversion

Bioprocesses – Biomolecules — (BioPromo) Axis

The BioPromo axis is managed by Prof. Eric Olmos and its primary concern is to develop design, and control bioprocesses for biomolecules in the field of biopharmaceuticals, nutraceuticals, energy, sustainable bio refinery, and bio-sourced production.

Product Engineering Axis

This is a transdisciplinary axis that combines concepts and methodologies of rheology, computational fluid mechanics, materials science, chemistry and physico-chemistry for the development of multi-structured products. The research axis is under the supervision of Prof. Philippe Marchal.

Processes, Reactors, Intensification, Membranes and Optimisation — (PRIMO) Axis

Prof. Jean-Marc Commenge is the head of this research axis. The PRIMO research group is fundamentally concerned with gas or liquid contactors, membrane and supercritical processes, intensified reactors and micro structured systems.

Kinetics – Thermodynamics – Energy — (CiTherRe) Axis

The research area carried in this team revolves around (i) pyrolysis kinetics, oxidation and combustion reactions (ii) thermodynamics, phase equilibria and the rational use of energy, and (iii) the thermochemical conversion of biomass for energy carriers. This work is also carried out in collaboration with Team ‘Greener’ a subgroup in the CITheRe axis. The research axis is supervised by René Fournet.

LIST OF ABBREVIATIONS AND NOMENCLATURE

G-G	Godbert-Greenwald	GC/MS	Gas Chromatography-Mass Spectrometry
MIT	Minimum Ignition Temperature	FID	Flame Ionisation Detector
RPM	Revolution Per Minute	RRF	Relative Response Factor
PSD	Particle Size Distribution	Tw	Minimum Ignition Temperature observed (°C)
daf	Dry ash-free basis	Tc	Minimum Ignition Temperature corrected (°C)
db	Dry basis	ISO	International Organisation for Standardisation
RT	Retention Time	IEC	International Electrotechnical Commission
TGA	Thermo—Gravimetric Analysis	dTG	derivative Thermo—Gravimetry
DSC	Differential Scanning Calorimetry	ΔP	Pressure change (mbar)
T	Furnace surface temperature (°C)	m	mass of organic dust (mg)

Abstract

Dust explosion of organic powders involves particles heating, pyrolysis, oxidation of pyrolytic gases and flame propagation. This work focused on the pyrolysis step, which can be rate-limiting during explosions. To better represent the pyrolysis stage, flash pyrolysis of four organic dust clouds (microcrystalline cellulose, wheat starch, oak and douglas fir) were carried out in a Godbert-Greenwald furnace from 700 to 900°C, at a heating rate of 1000°C.s^{-1}, a solid residence time between 150 and 250 ms and vapour residence time in less than 2 s. Tar condensates analysis verifies the production of levoglucosan as the major product for cellulose and wheat starch pyrolysis. Optic image analysis and residual volatile matter content determination with TGA confirmed low conversions of solid residues. The major gaseous components identified were H_2 (Hydrogen), CO (Carbon mono-oxide), CH_4 (methane), CO_2 (carbon dioxide) along with small yields of C_2H_2 (acetylene), C_2H_4 (ethylene) and traces of C_6H_6 (benzene). The effect of reactor temperature on gas compositions was studied. Experimental results indicated H_2, CO, and CH_4 increased with increasing reactor temperature whereas CO_2 showed a contrary trend. C_2H_4 and C_6H_6 also increased at elevated reactor temperature but C_2H_2 showed a similar trend as CO_2. Minimum Ignition Temperature (MIT) test results indicated the smallest hot surface temperatures that could be an ignition source for cellulose, wheat starch and oak dust explosions. Pyrolytic product analysis helped explain the pyrolysis behaviour of organic dust in the Godbert-Greenwald setup, a predictive model can be generated to predict the pyrolysis reaction rate of the dust in another work.

1.0. INTRODUCTION

The majority of powders used in industrial applications are combustible and pose a risk of a fire hazard if care is not taken. These combustible dust are finely divided particulates with the tendency of exploding when exposed to an oxidising agent (usually air) at a given concentration. They originate from organic sources (like wood, flour, starch, corn, etc), metals (aluminium, magnesium, etc) and inorganics in the course of materials handling, transportation, secondary finishing (grinding, polishing, cutting), crushing and blasting. Due to their tendency to cause fire hazards, they present a safety threat to wood-making and metal processing facilities, agriculture and food processing plants, chemical manufacturing plants (plastics, pharmaceuticals, etc) and any other dust-generating facility.

1.1 Background of Study

Dust explosion involves a rapid flame propagation and explosion through a cloud of combustible dust in contact with an oxidising agent (primarily air) and an ignition source with adequate energy [1]. During explosions, the combustible dust (finely divided particulate solid) act as a fuel source and its characteristics particle size are within 1 – 500 µm range [2]. According to researchers [1], [3], [4] dust explosion will only occur if the following conditions are present: combustible dust, oxidising agent, ignition source, dust dispersion and confinement. The first three conditions are perquisites to start and sustain fire hence they are collectively termed as the fire triangle which combines with dust dispersion and confinement to form an explosion pentagon [4] illustrated in Figure 2.

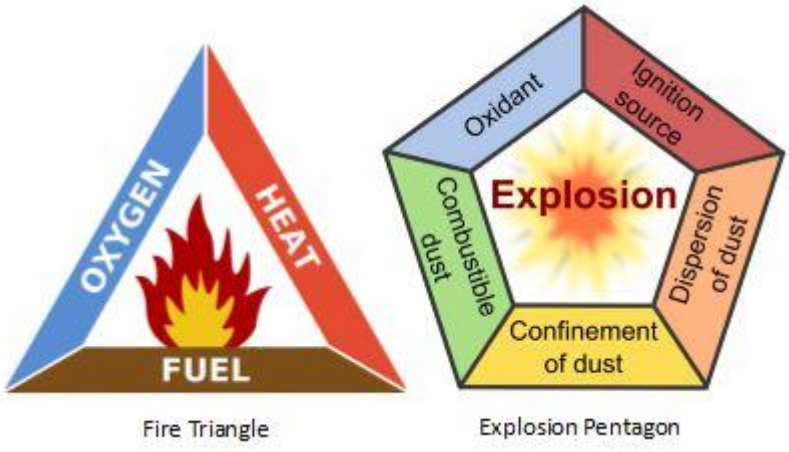

Figure 2: Dust explosion pentagon and fire triangle adapted from [5]

Combustible dusts are most likely dispersed from an unintentional powder release during equipment handling or several other industrial processes [1]. The release of such dust in the air or less known oxidising atmospheres like nitrous oxides or fluorine creates a dust/oxidant mixture ready to be combusted [5]. Based on the origin of the combustible dust the ignition source could vary from frictional heating, sparks, and static electricity to open flames. Once these elements are present the dust/oxidant mixture formed combust and creates an over pressure within a confined space which accelerates the flame propagation to transition into an explosion [1], [2], [4]. This poses threats to human lives, assets and the environment at large. For instance, in the mid-'90s, a dust explosion in a Chinese coal mine claimed the lives of 1594 people leaving 246 injured [6]. Again, in the early 2000s an imperial sugar refinery in Georgia, (United States) exploded leaving behind 50 casualties [7]. According to Yuan et al [3] as of 2012 over 2000 accidents worldwide were caused by dust explosions. Despite the significant advances made in research, the explosion from combustible dust still presents

a safety threat to processing industries hence understanding and identifying the key mechanism reactions is required to better model the risks [8].

The PErSeVAL research group over the years has contributed to scientific literature explaining the mechanisms involved in dust explosion and how to model the associated risk. For instance, Pico et al [9] used computational fluid dynamics alongside experimental procedures to investigate exhaustively the explosion severity of wheat starch pyrolysis gases hybrid mixtures compared to one phase explosion. In another work, Santandrea et al [10] studied the impact of nano particles characteristics on explosion severity and ignition sensitivities. Torrado et al [11] in their work assessed the effect of soot formation during dust explosion. Callé et al [12] also confirmed a decrease in explosion severity with increasing combustible dust particle size. Recently, Pietraccini et al [13] proposed a predictive model for organic dust explosion severity. In most of the work already studied not much has been done on the pyrolysis stage of dust explosion except the latter. During organic dust explosions, heated particles undergo pyrolysis, followed by the oxidation of pyrolytic gases produced and flame propagation [14]. Pyrolysis can be the rate-limiting step for organic dust explosion hence studying and understanding the pyrolysis stage is key to generating a predictive model of explosion severity for organic dust [15]. However, the flame temperature of organic dust could exceed 1000℃, with extremely short gas residence times (20 — 50 ms) and heating rates above $1000℃s^{-1}$ [16]. The aforementioned conditions can closely be attained only by flash pyrolysis. Given this, the present work aims to study the pyrolysis mechanism of organic dust explosion but will be centred towards flash pyrolysis. To achieve this, the following objectives will be carried out :

- Flash pyrolysis of various organic dust from 700 – 900℃ in a modified Godbert-Greenwald (G-G) furnace.
- Analysis of the pyrolysis product (gases, tars and chars) formed.
- Minimum Ignition Temperature (MIT) determination of cellulose, wheat starch and oak dust cloud.

Microcrystalline cellulose (Avicel PH-101), wheat starch (from Sigma Aldrich), oak and douglas fir harvested in Haut-Beaujolais (France) samples were used in this work.

1.2. Literature Review

This review is concerned with the pyrolysis mechanisms of various organic dusts. Pyrolysis is first explained, detailing the various products formed, types of pyrolysis, general and common reactors used. More emphasis on the review is placed on flash pyrolysis as it represents the pyrolysis stage of dust explosions. Afterwards, a succinct but comprehensive review of starch and cellulosic materials is given concluding with lignocellulosic biomass pyrolysis.

1.2.1 Pyrolysis

Pyrolysis in its etymological sense means decomposition by the action of heat; *"pyro"* (fire), *"lysis"* (cut) [17]. The process follows a thermochemical path, which degrades (~300 - 800°C) organic matter in the absence of oxidising agent into solid residues, liquid and gaseous products. The thermal decomposition is carried out in inert atmospheres usually with Nitrogen (N_2) or Argon (Ar) (with negligible concentrations of molecular oxygen) to avoid combustion reaction mechanisms from setting in [18]. Operating conditions such as temperature, heating rate and vapour residence time in a hot zone, have a tremendous effect on pyrolysis products, yields and compositions hence they can be optimised towards the formation of desired products. A physical phenomenon such as mass transfer within feedstock (biomass) also influences significantly the pyrolysis products especially char and tar yields

[19]. With heating rates reaching as high as 1000°C.s^{-1} at temperatures less than 700°C followed by rapid quenching of volatiles liquid formation is favoured minimising the production of solid residue and gaseous products [20]. With the same heating rate but increased temperature, (≥ 700°C) and short vapour residence time (< 2 s) gaseous product formation is enhanced and best represents the pyrolysis stage during organic dust explosions [20]. Slow heating rate (0.1 – 0.3°C. s^{-1}) at low operating temperature (< 700°C) and long vapour residence time (> 10 s) promote solid residue formation [21], [22]. The utilisation chain of pyrolysis products is shown in Figure 3.

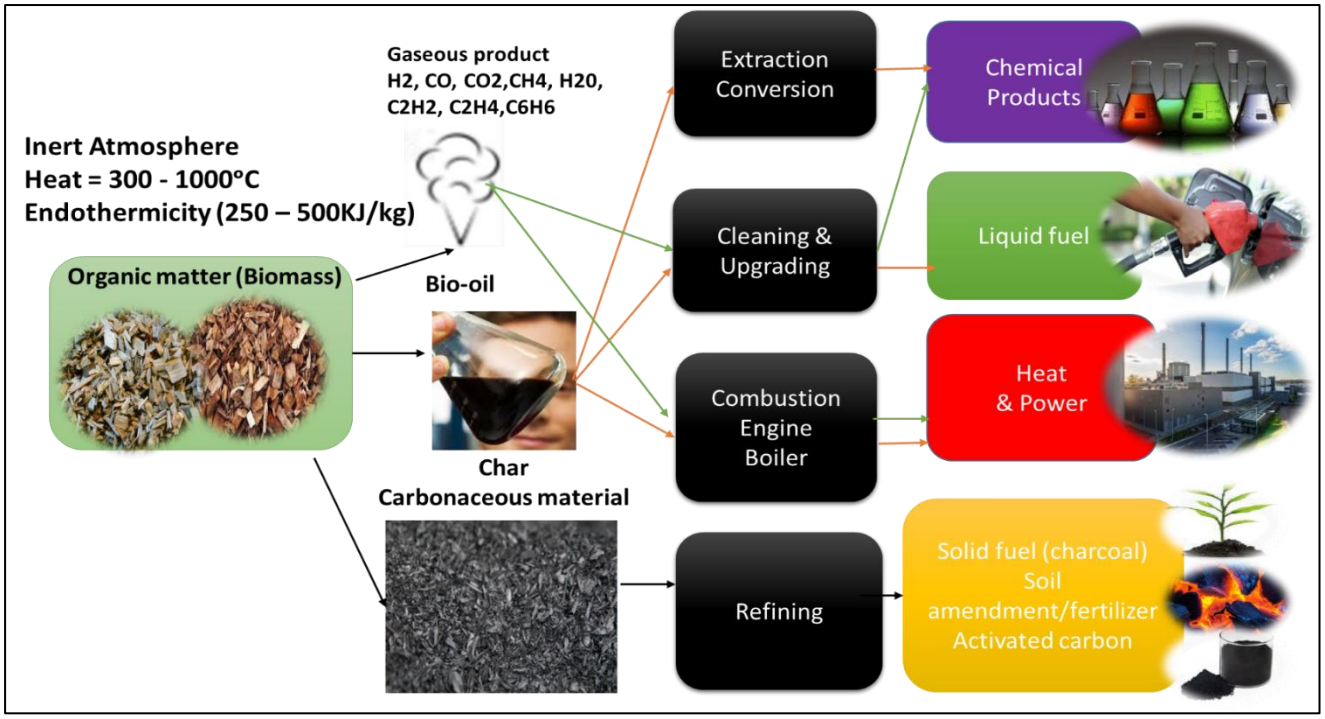

Figure 3: Pyrolysis Value chain adapted from [24]

1.2.1.1 Pyrolysis Products.

As discussed earlier, thermal degradation of organic matter via pyrolysis results in the formation of three distinct products namely: solid residue (char), liquid (tar/bio-oil) and gaseous products. The pyrolysis reactor type and feedstock used also have a strong correlation with the products formed.

1.2.1.2 Char

Char is the solid residue left after the pyrolysis process it comprises highly carbonaceous material and ash (inorganic residues). It is often referred to as bio-char if the pyrolysis feedstock is from biomass [23]. Char accounts for 5 – 40 wt.% of pyrolysis product depending on the pyrolysis conditions and corresponds to approximately 25% of the total energetic content of biomass feedstock [24]. As pyrolysis temperature increases gradually with increasing residence time, more H and O atoms are liberated from the biomass into the gaseous phase, and minerals get volatilised leaving behind a carbon-rich solid residue [26], [26].

1.2.1.3 Tar

Due to global challenges on fossil fuel depletion, increase in greenhouse gas emissions and the exponential demand in energy presently, the liquid fraction (tar) produced from biomass pyrolysis has

been an area of great interest for many researchers lately [27]. Tar commonly referred to as bio-oil is a dark-brown free-flowing but viscous liquid composed of intricate mixtures of oxygenated organic compounds (up 40 wt %), aromatic compounds (benzene, toluene, naphthalene) and a maximum of 30 wt % moisture content depending on the biomass feedstock used [28], [29]. Tar is collected when pyrolysis vapour (micron-sized droplets and polar molecules held together with water molecules) are quenched. The rate of cooling is critical as slow cooling would result in more viscous liquid formation, which could result in poor atomisation, high-pressure drop (increasing equipment cost), and equipment blockage [22]. The low heating value of bio-oil (~16 MJ/kg) and other reasons such as (i) high acidity (ii) high oxygen content (iii) low miscibility with hydrocarbons (iv) high viscosity and (v) phase separation renders it less desirable making cleaning and upgrading necessary if further valorisation (as a transportation fuel) is envisaged [23], [30]. Over 200 organic compounds can be derived from biomass bio-oil and they are generally grouped into five main classes of anhydrous sugars, phenols, derivatives of furan ring compounds, low molecular weight compounds and aromatics [23], [31], [32]. Table 1 presents a summary of the major compounds found in bio-oil.

Table 1: Bio-oil composition adapted from [18], [25]

Organic Groups	Chemicals
Acids	Formic, acetic, propanoic, hexanoic, benzoic, glycolic, 2-Butenic (Crotonic)
Esters	Methyl formate, methyl propionate, methyl crotonate, methyl n-butyrate, methyl acetate, butyrolactone, valerolactone
Alcohols	Methanol, ethanol, 2-propene-1-ol, isobutanol, 2-Propene-1-ol, Ethylene glycol
Ketones	Acetone, 2-butanone, 2-pentanone, 2-cylopentanone, 2,3-pentenedione, 2-hexanone, cyclo-hexanone, Dimethylcyclopentanone
Aldehydes	Formaldehyde, acetaldehyde, 2-butenal, pentanal, glyoxal, ethanedial
Phenols	Phenol, methyl-substituted phenols (2-Methyl phenol, 2,3-Dimethyl phenol, 2-Ethyl phenol)
Alkenes	2-Methyl propene, dimethylcyclopentene, alpha-pinene
Aromatics	Benzene, toluene, xylenes, naphthalenes, phenanthrene, fluoranthrene, chrysene
Nitrogenous Compounds	Ammonia, methylamine, pyridine, methylpyridine
Furans Furan,	Dimethyl furan, 2-furanone, furfural, furfural alcohol,
Guaiacols	2-Methoxy phenol, 4-methyl guaiacol, ethyl guaiacol, eugenol
Syringols	Methyl syringol, 4-ethyl syringol, propyl syringol
Sugars	Levoglucosan, glucose, fructose, d-xylose, d-arabinose, 1,6-Anhydroglucofuranose
Miscellaneous oxygenates	Hydroxyacetaldehyde, hydroxyacetone, dimethyl acetal, acetal, methyl Cyclopentenolone

Considering the high heating and extremely rapid heating rate ($\geq 1000℃s^{-1}$) during organic dust explosions, the overall tar that may be produced is significantly low [20]. The various components of bio-oil (tar) illustrated in Table 1.0 vary with increasing heating rate and temperature due to differences in thermal stability. At elevated temperatures like in the case of flash pyrolysis thus organic dust explosions, anhydrosugars (dominated by levoglucosan) formation is slightly favoured. Furans, aldehydes and ketones follow in a decreasing order but are of lower concentrations like the remaining tar compositions combined [35,36].

1.2.1.4 Gaseous Product

Pyrolysis gaseous products are non-condensable gases (permanent gases) collected after bio-oil vapour condensation [17]. The gas composition comprises varying fractions of CO_2, CO, CH_4, H_2, relatively low yields of C_2H_6, C_2H_2, C_2H_4, water vapour and traces of C_6H_6 [17], [23], [35]. Increasing the pyrolysis temperature and heating rate favours permanent gases formation. Wei et al [36] investigated the effect of temperature on gas composition, char of pyrolyzed agricultural residues (maize straw, rice straw, cotton straw, and rice husks), and found a significant rise in gas yield as temperature increased ($600 < T_p \leq 1000$). Permanent gas yield increase with increasing temperature can be attributed to two main reasons (i) faster rate of pyrolysis vapours cracking [37] and (ii) secondary char (solid residue) decomposition [36]. Pyrolytic gases have sufficiently good heating value (17 — 19.5 MJ/kg) which can be combusted to power pyrolysis plants, gas engines, and turbines [38].
Just like bio-oil, pyrolysis gases require a cleaning step to prevent SO_2, NO_X and HCl pollution during further valorisation [23], [38]. Unfortunately during combustible dusts explosion, pyrolytic gases produced rather ignite in the surrounding atmosphere increasing explosion severity and violence [2],

1.2.2 Classification of Pyrolysis Procedure

Thermal decomposition by pyrolysis in process industries has been in existence for a long. Solid fuel (charcoal) production from biomass feedstock pyrolysis initially was the main product until recently where advancement in the technology has contributed to the production of value-added chemicals (gaseous & chemical product) from the thermochemical valorisation route [23]. As discussed already, operating conditions influence products formation hence pyrolysis classification is done based on such conditions particularly the heating rate, temperature and vapour residence time. Pyrolysis can broadly be classified into four[39] as described below.

1.2.2.1 Slow Pyrolysis

Slow or classical pyrolysis is one of the oldest techniques used for biochar production [17]. The feedstock (biomass or organic matter) is heated between $\sim 300 - 500℃$ at a low heating rate of 0.1 – $0.3℃.s^{-1}$ and long residence time to facilitate secondary reactions in the volatiles leaving behind adequate carbonaceous (char) material with a corresponding low tar and gas yield [23].

1.2.2.2 Intermediate Pyrolysis

The reaction temperature range for intermediate pyrolysis is between $\sim 400 - 500℃$, a heating rate between 1 and $10℃.s^{-1}$ with intermediate feedstock residence time up to 10 minutes [23]. Yang et al [40] in their work identified this type of pyrolysis to be suitable for several feedstocks ranging from biomass, municipal and de-inking sewage sludge. Bio-oil yield from this type of pyrolysis could get as high as 50 wt % with equal weight distributions for gases and chars (25 wt %) [17].

1.2.2.3 Fast Pyrolysis

This pyrolysis technique has been developed to maximise the bio-oil yield. To achieve this, the following operating conditions are carefully controlled [41]; (i) finely ground feedstock (ii) high heating rate (10 - 1000℃.s^{-1}) (iii) moderate temperatures ($\sim 400 - 600$℃), (iv) short volatiles residence time (v) and rapid cooling of pyrolysis vapour. At optimum operating conditions the 3 major pyrolysis products are obtained in the following proportions; 60 – 75 wt% bio-oil, 10 – 20 wt% gaseous product and 15 – 25 wt % char [42].

1.2.2.4 Flash Pyrolysis

Flash pyrolysis is also known as very fast pyrolysis can be identified by its rapid heating rate (1000℃.s^{-1}), high reaction temperatures (> 650℃) and extremely fast vapour residence time (10^{-2} s). For efficient heat and mass transfer at the aforementioned conditions, the feedstock (biomass) should be small in a $\sim 100 - 500$ µm particle size range due to the characteristics heating time of the particles [43]. Pyrolysis under these operating conditions are not easy to come by as such only a few experiments have been performed up to date. Zanzi et al [44], [45] in their work showed that pyrolysis at higher reaction temperature (800 - 900℃) leads to the formation of predominantly gaseous products with low tar and char yields. Commandre et al [46] confirmed this in their work where flash pyrolysis of wood resulted in about 76 wt % gases, 7 wt % char and 1.5 wt % tar formation. The main gaseous species obtained during flash pyrolysis of biomass feedstock are hydrogen (H_2), Carbon mono-oxide (CO), carbon dioxide (CO_2), methane (CH_4) and other hydrocarbons, all but CO_2 tends to increase with increasing temperature [44]–[46]. The H_2/CO and CO/CO_2 ratios have been found to increase with increasing temperature [47]. As discussed earlier, flash pyrolysis operating conditions are close to an organic dust explosion. As such, flash pyrolysis experiments were carried out in a non-conventional pyrolysis reactor capable of reaching extremely rapid heating rates (1000℃.s-^{1}). A summary of the various types of pyrolysis and their operating conditions is given in Table 2.

Table 2: Comparative Summary of Pyrolysis Techniques with operating conditions (Adapted from [25], [46], [48]).

Properties	Pyrolysis Techniques			
	Flash	Fast	Intermediate	Slow
Temperature (°C)	700 — 1000	400 — 600	500 — 600	300 — 500
Heating rate(°C/s)	1000	10 — 1000	1 — 10	0.1 — 0.3
Vapour residence time (s)	≤ 0.5	<2	10	>10
Char yield (wt %)	5 — 17	15 — 25	25	20 25
Bio-oil)yield (wt %	0.8 — 1.5	60 — 75	50	25 35
Gaseous product (wt%)	60 — 80	10 — 20	25	30
Flux density (W/m^2)	> 10^6	> 10^4	> 10^4	<10^3

1.2.3 Pyrolysis Reactors

This part of the review focuses on the most commonly used biomass pyrolysis reactors. The majority of the current reactors are optimised for maximum liquid fuel (bio-oil) production [17]. In the reactor designs, heat transfer to the feedstock (biomass) employing radiation and convection from the hot reactor surfaces to the particles and conduction within the particles themselves are of primary importance as they influence the formation of the overall product [23]. Current reactor designs vary majorly in two key areas; (i) the mode of feedstock feeding and (ii) the heat transfer method. For instance, in fixed bed reactors, organic matter (biomass) are fed upwards or downwards, pyrolysis vapour produced is collected and later quenched thanks to inert carrier gases [48]. For rapid and homogenous heating of the biomass, some reactors employ a hot stream of gases to fluidise inert sand materials which in turn pyrolyzes the feedstock as done in team Greener [49]. For reasons of improved efficiency other reactors co-feed biomass with sand which get pyrolyzed as it moves along a hot auger screw [50] or in a rotating cone [39]. Other reactors pyrolyze biomass under vacuum avoiding the use of carrier gas [51] or microwave heating technology [52]. A comparative summary of various pyrolysis reactor technologies is given in Table 3**.** In this work, a modified furnace (non-conventional reactor) similar to a free-fall reactor was used for flash pyrolysis experiments.

Table 3: Comparative Overview of Pyrolysis Technologies

Technology	Description	Pros (+) & Cons (-)	Company/Lab (Status)	References
Bubbling Fluidised bed (BFB) (500-800°C)	• High heat transfer with preheated sand •Residence time of vapour and biomass controlled by fluidization gas • Bio-oil yield ~ 70-75 %	**+:**High quality bio-oil, simple design and operation, precise temperature control **-:** Small biomass particles(2-3 mm), Requires external heat sources	RAPSODEE, Albi LRGP, Nancy RTI, Dynamotive, Aston, Hamburg, Fortum (Commercial/Demonstration)	[24][53][54]
Circulation Fluidized Bed (CFB) (450-800°C)	•Similar to BFB, but the residence time for char & gas is the same unlike BFB •Hot sand circulating between combustor and pyrolyser •Heat produced by combustion of char	**+:**High flow rate, already used for large volume in the petroleum industry **-:** Heat transfer less efficient than BFB, Abrasion, Small particles in bio-oil	Ensyn, VTT, Fortum, Metso (Commercial/ Demonstration)	[24], [53][55]
Rotating Cone (300-600°C)	Preheated sand in contact with biomass in a rotating cone	**+:**Compact system, No need for fluidization gas **-:** Complex process, Requires small particle size,	University of Twente BTG-BTL (Commercial)	[24][56]

Table 3: Continued

Technology	Description	Pros (+) & Cons (-)	Company/Lab (Status)	References
Ablative Pyrolysis (500-700°C)	•Heat transfer by direct contact of biomass particles with hot reactor under pressure applied by mechanical or centrifugal force •Liquid film formation with pyrolysis products then evaporated •Bio-oil yield~ 60-75 %	**+:**Big particles, No need for fluidization gas **-:** Complex process, limited by the thermal power delivered (energy input problem), Difficult up-scaling	NREL (Vortex), Aston, Pytec/Germany (Demonstration)	[24]
Auger Screw Pyrolysis (400-600°C)	•Hot sand and biomass mixed in a screw •Biomass moves using a screw	**+:**Compact and mobile technology, Reduction of transportation/storage costs, No need for fluidization gas	Renewable Oil International, ABRI Tech, KIT (Demonstration	[24], [53]
Vacuum Pyrolysis (200-400°C)	•Biomass moves by gravity and by rotary drag through multi-cells pyrolysis •Induced thermal decomposition of biomass under pressure •Bio-yield= 35-40 % (450°C, 15kPa)	**+:** Big particle size, No need for fluidizing gas; No particles in bio-oil **-:** Low heat transfer, Low bio-oil yield, High cost (vacuum pump),	Pyrovac, Laval University Canada	[51]
Conical spouted bed (350-700°C)	•Preheated cyclic moving sand and feedstock are in contact within a conical bed.	**+:** Easy to construct and design High heat and mass transfer rate between phases. Good inter-particle contact Suitable for a wide range of feedstock (biomass, polymers, municipal solid waste) **-:** Requires a fluidising agent (N_2)	Ikerlan (Spain) (Pilot plant)	[24], [57]

As already discussed in Chapter 1.2 the rest of the review captures the pyrolysis mechanism of samples used in this work beginning with cellulose, starch and lignocellulosic biomass (oak and douglas fir). Sample sources and characteristics are discussed later in Chapter 3.1

1.2.4 Pyrolysis of Cellulosic Materials

Cellulose is a polymeric material present in woody and grass biomass contributing to the cell walls strength and rigidity. It consists of cellobiose, a glucopyranose repeating unit formed from glucose anhydrous residues held in place by β (1→4) glycosidic bonds [23]. Its strong Intra and inter hydrogen molecular bonding results in the formation of a predominantly crystalline structure leaving small room for amorphous regions, this makes thermal valorisation routes more appropriate for cellulosic materials [23][58]. The molecular formula of cellulose is represented by $(C_6H_{10}O_5)n$ [59]. Figure 4 illustrates the chemical structure of cellulose.

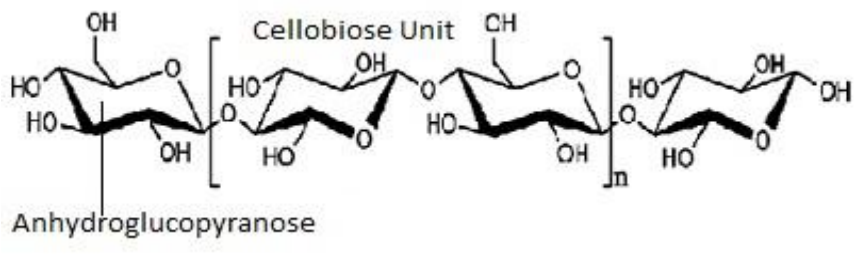

Figure 4: Chemical Structure of Cellulose [44]

Cellulose pyrolysis is an endothermic process that results in the formation of complex volatiles [60]. During cellulose thermal degradation, there is

(i) removal of absorbed humidity (25 - 150℃) [61]
(ii) splitting off of structural water, formation of free radicals, carbonyl, carboxyl, hydroperoxide groups, CO, and CO_2 (150 - 240℃) [61], [62]
(iii) thermal splitting of glycosidic bonds resulting in the formation of pyrolysate liquid mainly composed of levoglucosan accompanied with the release of anhydrosugars, oligosaccharides and extra water, (240 - 400℃) [61], [62]
(iv) the formation of graphite-like structures (beyond 400℃) [61].

As cellulose get heated the long-chain molecules are decomposed into activated cellulose followed by depolymerisation and fragmentation [62], [63]. Depolymerisation of activated cellulose gives rise to anhydrosugars (mainly levoglucosan), furans, cyclopentanones whereas fragmentation on the other hand results in the formation of linear carbonyls, alcohols and esters [64]. The decomposition mechanism involves glycosidic bond cleavages first the breaking of C—O weaker bonds followed by C—C bonds [60]. The discussed degradation mechanism for cellulose is a global overview as several degradation mechanisms have been proposed [44], [45], [65]

1.2.5 Starch Pyrolysis

Starch is the third most abundant biopolymer only behind cellulose and chitin. It is a derivative from naturally occurring energy storage crops like corn, potatoes, wheat, rice, tapioca, sorghum, arrowroot, and sago palm [66]. Starch is broadly classified into three groups based on its origin; Type A (from cereals), Type B (from tubers, fruits and stem) and Type C (from legumes, and roots). In this work, a Type A starch (wheat) with a parallel double helix structure was used [67]. Starch and Cellulose share a similar chemical structure but vary in geometry. The glucopyranose repeating units $(C_6H_{10}O_5)n$ are linked by β (1→4) glycosidic bonds in cellulose and α (1→4) glycosidic bonds in starch causing the

starch to generally decompose at slightly lower temperatures [66], [68]. The two major constituents of starch are amylose (20 – 30 %) and the α (1→6) branched amylopectin component (70 – 80 %) [66], [69]. The amylose component is predominantly found in the amorphous regions whilst the branched amylopectin accounts for starch crystallinity [66]. The chemical structure of wheat starch is illustrated in Figure 5

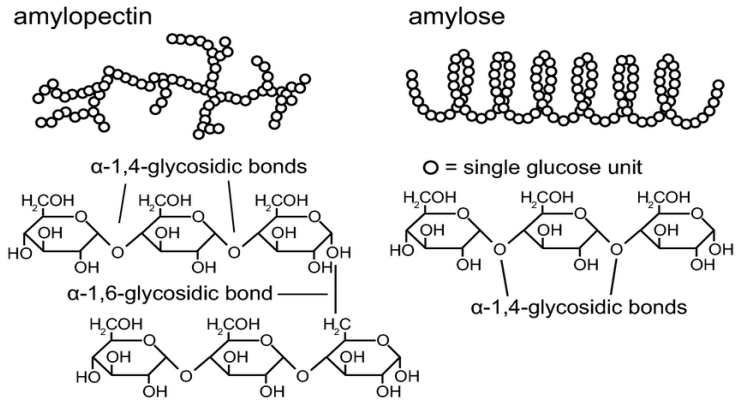

Figure 5: Chemical structure of the major constituents of starch

The major steps involved in starch pyrolysis under inert atmosphere involve [69];

(i) dehydration
(ii) splitting of hydroxyl groups
(iii) thermal decomposition of organic compounds,
(iv) carbonization.

After the water evaporation step, small quantities of the loosed branched amorphous regions degrade at low activation energy followed by the thermal degradation of the crystalline segments at higher activation energy [68], [70]. The decomposition products obtained from starch pyrolysis are generally grouped into three (i) gaseous products (ii) viscous syrup (pyrolytic condensate) and (iii) char [71]. The gaseous products comprise Carbon monoxide (CO), Methane (CH_4), Carbon dioxide (CO_2), and Hydrogen (H_2) whereas the pyrolytic condensate is predominantly Levoglucosan (1 – 6 anhydro β-D glucopyranose) and fractions of water, acids, and aldehydes [72]. Coking is often associated with starch pyrolysis due to delayed depolymerisation caused by rearrangement reactions of stabilised residues in starch's amorphous regions [68].

1.2.6 Lignocellulosic Biomass Pyrolysis.

Lignocellulosic biomasses are plant materials that comprise mainly of three polymers; cellulose, hemicellulose and lignin. They also contain traces of minerals and extractives in varying amounts just like the three basic components already mentioned. [17], [23], [70]. Table 4 gives a global proportion of cellulose, hemicellulose and lignin present in woody biomasses.

Table 4: Comparative Overview of Pyrolysis Technologies

Biomass Type	Cellulose (wt.%)	Hemicellulose (wt.%)	Lignin (wt.%)
Softwood (Douglas)	35 — 50	25 — 30	27 — 30
Hardwood (Oak)	45 — 50	20 — 25	20 — 25

Due to the varying nature of biomass, it is safe to say two biomass feedstocks cannot be pyrolyzed in the same way however a global representation of the biomass pyrolysis stage can be realised [23] as follows;

(a) initial evaporation of water from the feedstock (drying)

(b) quick depolymerisation and volatilisation

(c) sustained organic matter degradation, and carbonization

(d) secondary and tertiary reactions between pyrolysis products formed.

To better understand the overall biomass pyrolysis, it is important to know the behaviour and role of each component present in the biomass. As a result, this part of the review focuses on hemicellulose, lignin, minerals and extractives pyrolysis since cellulose pyrolysis has already been discussed in Chapter 1.4.1.

1.2.6.1 Hemicellulose Pyrolysis

Hemicellulose consists of short-chain heteropolysaccharides amorphous branched structure and few sugars with a general molecular formula $(C_5H_8O_4)n$ where n (degree of polymerisation) is ~ 200 [23][70]. Hemicellulose is known to contain higher amounts of moisture unlike lignin, this contributes to its low pyrolytic degradation tendency within the temperature range of 230 — 400℃ [73]. Another reason for the low pyrolytic degradation temperature in hemicellulose is due to its main constituent, xylan shown in Figure 6. The pentosan components present in xylan increases the ease of hydrolysis and dehydration reactions rendering the entire hemicellulose structure less thermally stable[74].

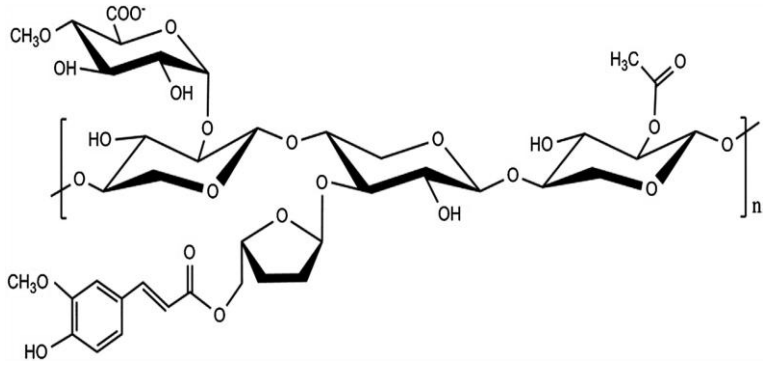

Figure 6: Structure of xylan [25]

Hemicellulose pyrolysis gives rise to the following pyrolytic condensate products; water, acids (formic, acetic, propanoic), ketones (hydroxy- 1-propanone, hydroxy-1-butanone), methanol, aldehyde (2-furfuraldehyde, acetaldehyde), isomers of dianhydro xylose and a large amount of carbon dioxide (CO_2) in its gaseous composition [75][76].

1.2.6.2 Lignin Pyrolysis

Lignin is characterised by an amorphous three-dimensional polymeric structure composed of the following phenyl propane units; p-hydroxyphenyl (H), guaiacyl (G), and syringyl (S) units formed by dehydrogenation polymerisation of coumaryl alcohol, coniferyl alcohol and sinapyl alcohol respectively making its decomposition uneasy[77]. The biosynthesis of lignin involves the radical coupling of monomers for the formation of racemic, cross-linked, phenol polymers, which gives rise to the varying lignin content among various lignocellulosic biomass and different structure within the same biomass [78]. Lignin contains some functional groups such as methoxyl, carbonyl, carboxyl, and

hydroxyl groups connected to either an aliphatic or aromatic moiety in varying amounts giving an added explanation to the different lignocellulosic biomass lignin content [79]. Liu et al [80] in their work established that almost 50 % of the lignin matrix is composed of aromatic compounds making it hydrophobic. The known linkage patterns in lignin can be grouped into six classes namely, β—O—4 ether bonds (dominant bonds), β—5 phenylcoumaran bonds, β—β' pinoresinol, diphenyl ether 4—O-5', β—1' diphenylmethane, and 5—5' bond [81]. The proportion of H/G/S units in lignin largely depends on the biomass species. Generally, softwood lignin is composed mainly of guaiacyl (G) phenolics with little amount of p-hydroxyphenyl (H) units and close to zero syringyl phenolics (S) units whereas hardwood lignin on the other hand, contains approximately equal amounts of guaiacyl (G) and syringyl (S) units[87,89].

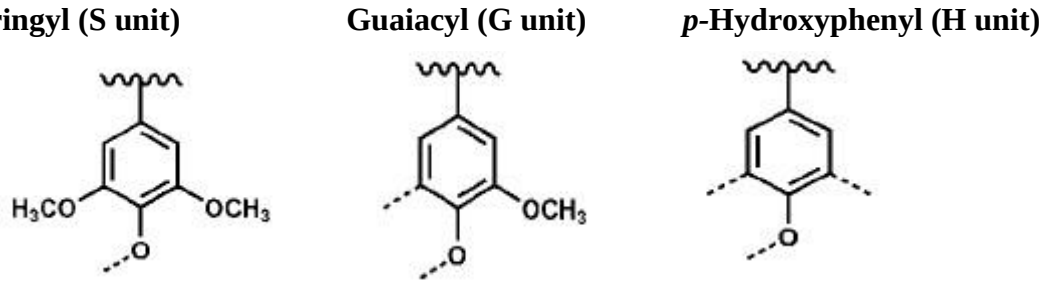

Figure 7: The primary monomeric lignin units [86].

Patwardhan et al [83] examined pyrolysis products of lignin and identified the following pyrolytic condensates as the major compositions; phenol, 4—vinyl phenol, 2—methoxy—4-vinyl phenol, and 2,6—dimethoxy phenol. They also confirmed that alkylated phenols and gaseous products yield increased with temperature whilst methoxylated phenols as well as char yields decreased. The pyrolytic degradation temperatures of the three major constituents of biomass can be highlighted as; 230 — 315℃ for hemicellulose, 315 — 400℃ for cellulose and a wide range of temperature for lignin (over 500℃ — 900℃) [17]. This thermal behaviour can be seen in the work by Jin et al [84], where hemicellulose (xylan), cellulose and lignin were analysed in a TGA from 50 — 700℃ at a heating rate of 10℃ in an inert atmosphere.

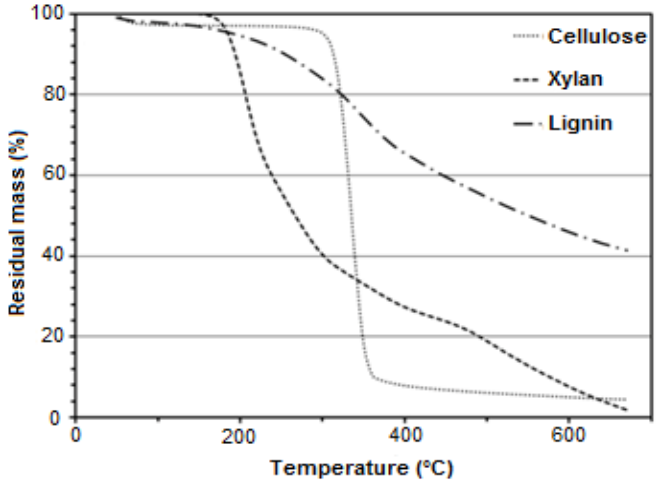

Figure 8: Fast pyrolysis TGA curves for major biomass constituents [88]

1.2.6.3 Extractives and Minerals Pyrolysis

Small amounts of extractives are present in all lignocellulosic biomasses in addition to cellulose, hemicellulose and lignin. However, extractives are non-structural components of the biomass which do not form part of the cell wall [70]. The components of extractives are broadly grouped into three;

aliphatic compounds (waxes and fats in the form of fatty acids attached to glycerol), terpenes and terpenoids (source of odour), and phenolic compounds [17], [70]. Due to their low yields in biomasses, extractives are not accounted for during pyrolysis yet they influence the thermochemical valorisation routes and pyrolysis products particularly bio-oils [70], [85]. The thermal degradation temperature of extractives is considerably low 205℃ compared to hemicellulose (270℃), cellulose (370℃) and lignin (> 370℃) [86]. The presence of extractives has been found to increase biomass component activities and enhance structural compound decomposition during pyrolysis [86]. For instance, biomass with high extractive content has improved liquid yield (high levoglucosan) but low char and gas yields whereas extractive-free biomass are known to produce a higher amount of CO_2, and CO [87], [88]

Biomass (woody) contains a small number of inorganic minerals up to 4 wt % [70][89]. These minerals consist of potassium, calcium, sodium, magnesium, silicon (Si), phosphorus (P), sulphur (S), chlorine (Cl), and some traces of heavy metals (zinc, molybdenum, iron, cobalt, etc) depending on the biomass origin [70], [90]. The mineral compositions vary based on the biomass type and they are often found in the ash as oxides of calcium (CaO), silicon (SiO_2) or potassium (K_2O) etc or amides chemical groups in the bio-oil [70], [91]. The majority of these inorganics are retrieved in the chars formed after pyrolysis and despite their small proportions they do exert a good catalytic effect on the pyrolysis mechanism and the products formed [70]

1.2.6.4. Cellulose, Hemicellulose and Lignin Interaction during biomass pyrolysis

Cellulose, hemicellulose and lignin interaction during biomass pyrolysis can be examined based on the fractions, characteristics and compositions of pyrolytic products formed [77]. While some researchers claim there is little or no detectable interaction between the three major components of biomass during pyrolysis, others argue some degree of interaction does exist because the simple superposition of the individual components does not explain lignocellulosic biomass behaviour [92], [93]. For instance, pyrolysis of spruce wood, beechwood, huzle nut and olive husk resulted in ~ 45 % of levoglucosan yield although the cellulose contained in the lignocellulosic biomass tested could have yield close to 50 % levoglucosan. Interactions between the three major biomass constituents suppressed the formation of levoglucosan and instead enhanced 5-methyl-furfural formation [94], [95]. The work by Hosoya et al [96] further confirms that the presence of lignin enhances micro molecule formation (5-methyl-furfural) rather than macromolecular products (levoglucosan) during cellulose degradation. Cellulose on the other hand inhibits char formation of lignin but promotes lignin decomposition into phenols. Greenhalf et al [97] found out that the maximum thermal decomposition rate is lower for biomass with higher lignin content which happens to be the case for the Douglas (Lig: 34.4 wt %) and oak (Lig: 24 wt %) samples used in this work [98]. Similarly, aldehydes components in this work are expected to be higher for oak samples with a higher cellulose content than douglas based on the prediction by Chen et al [99]. This elucidates claims by researchers who agree on cellulose, hemicellulose and lignin interaction during biomass pyrolysis.

2.0. EQUIPMENT AND INSTRUMENTATION

2.1. Godbert-Greenwald (G-G) Furnace

The main equipment used for flash pyrolysis and Minimum Ignition Temperature (MIT) determination is presented. The G—G furnace dates as far back as 1935, a Great Britain and USA cooperation between Godbert (Brit) and Greenwald (American) to develop a laboratory-scale method that could determine if coal dust or a mixture between coal dust and inert dust could explode [100]. The work of Godbert and Greenwald was an improvement of the method already developed by Godbert and Wheeler in 1925 [101]. Vertical Tubular furnace used by the German researchers Holwartz and Von Meyer (1891), later by French researchers Taffanel and Dur (1911) in their work became forerunners to the present-day G—G furnace. Presently, the G-G furnace is the most known apparatus for determining standardised Minimum Ignition Temperature (MIT) tests for dust clouds according to ISO/IEC 80079-20-2. MIT test is often carried out on organic dust to determine the minimum temperature that could cause ignition and subsequent explosion when the dust comes in contact with hot surfaces. Changes were made to the original set-up for flash pyrolysis experiments, the changes made are highlighted later in this chapter. The main components of the G-G furnace are the gas tank with an approximate volume of 500 cm^3, a dust holder/chamber with a maximum capacity close to 600 $c\,m^3$ [102] and the heating chamber. The gas tank is connected to tubing that allows gas to flow through the G-G setup. A three-way ball valve with one inlet and two outlets is fitted to the exit of the tubing connected to the gas tank. One outlet of the three-way valve is screwed to a pipe that serves as the pathway for purge gas while the other outlet is attached to the dust holder/chamber. The dust holder/chamber is held in place by a rubber band connected to a glass adaptor screwed unto the heated chamber. Other auxiliary instrumentation includes:

1. Gas supply system
2. Open and close valve
3. Gas pulse valve
4. Graphite Gasket
5. Temperature controller and dispersion unit.

The heated chamber consists of a furnace mounted on a tripod. At the centre of the furnace is a cylindrical refractory material with a height of about 20 cm and an external diameter of 3.4 cm. The refractory tube is heated from its external walls by nichrome windings concentrated at the ends of the tube to minimise the effect of temperature gradient [100]. The refractory vertical tube is thermally insulated with vermiculite encapsulated in a cylindrical sheet for safety reasons. The height, diameter and volume of the heated chamber are 0.22 m, 0.20 m, and 6.91×10^{-3} m^3 respectively. Two K-thermocouples (Ø 0.1 mm) were clamped to the tripod and inserted from the bottom of the chamber and positioned against the tube walls for temperature measurements. The thermocouples are connected to a Eurotherm 2116 temperature controller unit (Chilworth Technology, Southampton England) with a maximum temperature of 1000°C. The temperature control unit allows easy setting of over temperature set point and reading of current temperature at the display unit. The unit is fitted with a dispersion button connected via a gas pulse valve to the gas tank of the G-G set up which allows samples to be dispersed during experimental procedures. The G-G setup is illustrated in Figure 9 below.

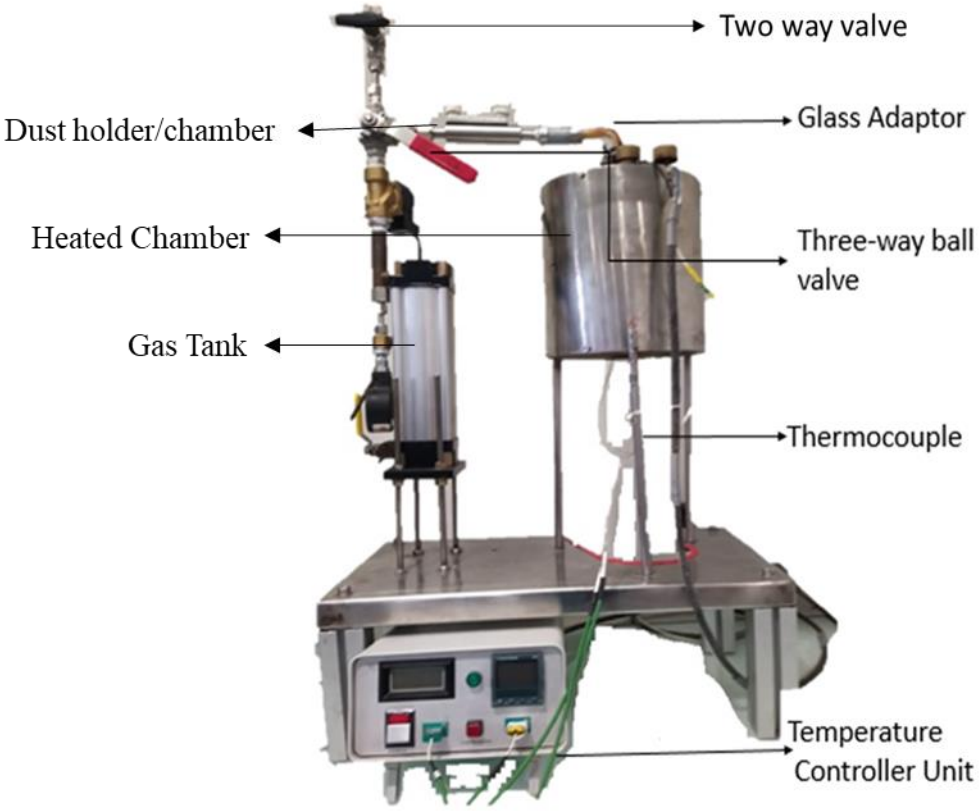

Figure 9: The Godbert-Greenwald (G-G) furnace

2.2. Modifications made on the Godbert-Greenwald furnace.

Changes to the original design of the G-G setup were recently (2020) made by the PErSeVAL research group at LRGP to accommodate high-temperature flash pyrolysis products. The following are the modifications made:

(1). A capped vertical tube with a height of 280 mm and an external diameter of 33.7 mm was inserted in the central cylindrical refractory material of the heating chamber. The cap, with thickness, external and internal diameters of 20 mm, 50 mm and 27.30 mm respectively allowed the tube to rest on a gasket fitting on top of the heating chamber. This leaves about 4 mm of the vertical tube out of the heating chamber and half of this length is the male thread fitted to the condensation chamber as shown in Figure 10.

(2). The glass adaptor was replaced by a metallic tube/elbow with better resistance to thermal and mechanical failures at higher temperatures. The thermocouples were detached from the tripod and repositioned in the setup. One thermocouple was inserted in the Inconel vertical tube through a groove created on the side of the metallic tube/elbow sealed with olive in Teflon to avoid gas leaks. This records temperature measurements in the heated chamber. The other thermocouple was wound around the metallic tube/elbow for safety purposes.

(3). A condensation chamber that consists of an Inconel tube, solid trap and a u-shaped tube was screwed to the bottom of the vertical tube through a female thread adapter was made to help capture tars. The Inconel tube is 100 mm long with 25.4×21 mm internal and external diameters respectively. A 30 mm clearance exists between the base of the Inconel tube and the solid trap lined with two metallic sieves for trapping solid residues. The end of the solid trap is screwed to a U-shaped tube with an external diameter of 8 mm, curvature length and radius of 63 mm and 25 mm respectively. The

welded Aluminium—6061 tube consists of 100 mm long cylindrical bars on both sides screwed to the condensation chamber's curved region. The upper end of the U-shaped tube is extended by some 40 mm radius of curvature and fastened to the product gas exit.

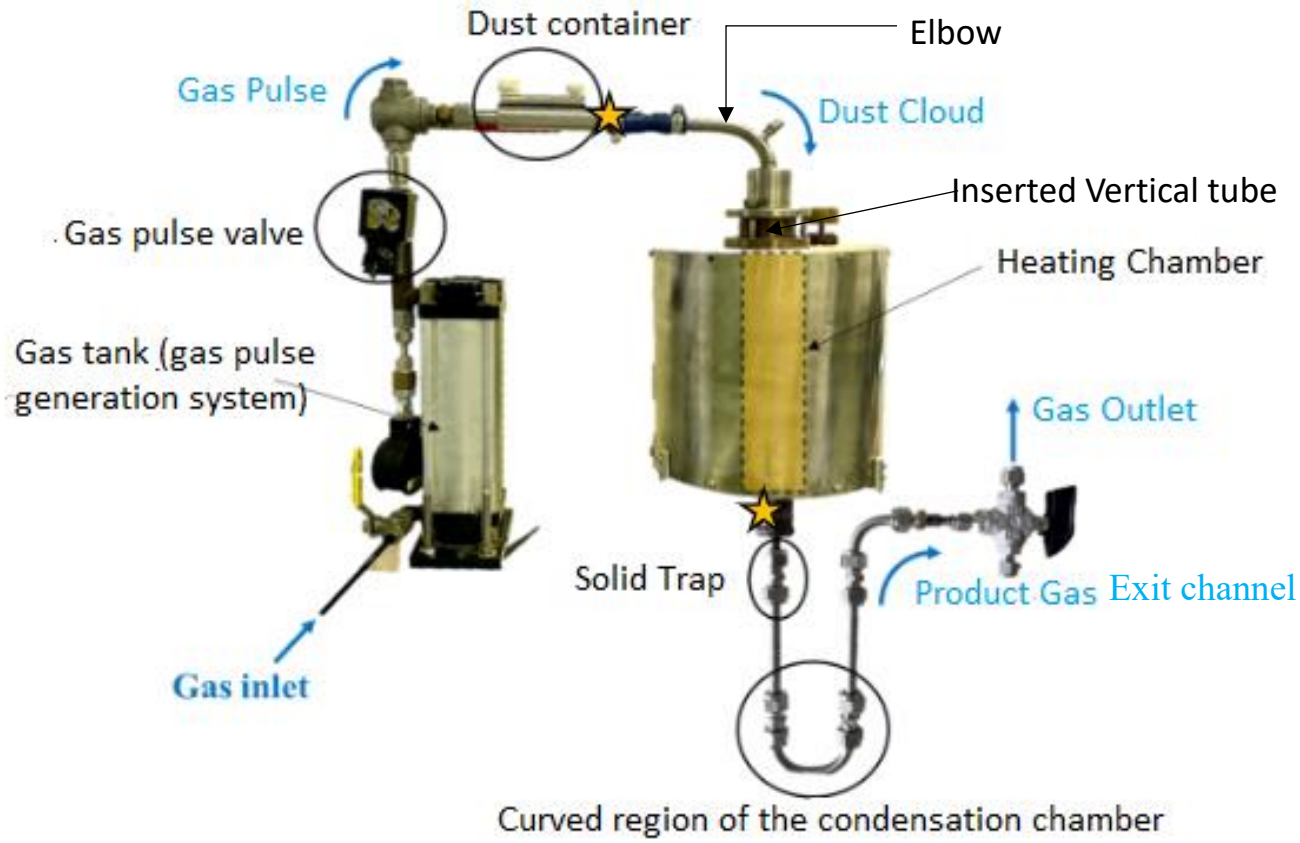

Figure 10: The Modified Godbert-Greenwald Furnace [107]

The yellow stars indicate where the in-situ particle size distribution (PSD) analysis was carried out.

2.3 Mode of Operation of the G-G Furnace

2.3.1 Preliminary Cleaning Step

Before a test, a preliminary cleaning step is carried out on the modified G-G furnace. The entire setup was taken apart and cleaned to get rid of sample residues from the previous test. Setup reassembling immediately followed this. Carrier gas (Argon) was allowed to flow through the gas lines into the gas tank (gas pulse generation system) and the product gas exit channel with the help of a Y-shaped splitting junction. The two-way valve was adjusted to allow carrier gas flow from the product gas exit channel through the condensation and heated chambers, elbow, dust holder, three-way ball valve (inclined at 45°) and finally out of the setup via an outlet of the three-way ball valve. With this configuration, flushing the setup with Argon at 1.4 bar was realised and continued for a 5-minute duration getting rid of gases and moisture. The setup configuration is represented in Figure 11.

2.3.2 Sample Dispersion Step

After the gas flushing step, leaks were checked using the soap-bubble technique. With the Argon still flowing, the two-way valve was closed while the three-way ball valve was adjusted parallel to the dust holder. Once pressure leakages were detected the respective screws, joints, gasket fittings, and/or olive

in Teflon were retightened until no leaks were confirmed, else a blank argon test was carried out. The temperature controller unit was turned on and allowed to reach the set temperature point within 15 – 20 minutes. The setup configuration for the leak test was slightly adjusted by turning the product gas exit channel valve upwards allowing carrier gas to flow in a reverse direction to the path already described during the preliminary cleaning step. This puts the set-up in sample dispersion mode as shown in Figure 11. Argon gas was dispersed about 10 times to get rid of any residual air or moisture. A vacuumed Tedlar sampling bag was attached to the gas outlet tube followed by a Blank Argon test to confirm the absence of air in the set-up. With the G-G setup in the sample dispersion mode, the gas tank valve was opened and later closed to pressurise the setup with Argon at 1.4 bar. The Argon pressure was measured with the digital pressure gauge attached to the gas tank. Once the pressure was attained, the pressurised carrier gas was dispersed with the help of the dispersion button and later collected in the Tedlar sampling bag. Oxygen and nitrogen gas concentrations in the collected gas were analysed in a micro—GC with maximum allowable concentrations of 0.5 and 2 % respectively. If the threshold is not exceeded the set-up was deemed to be ready for flash pyrolysis experimental procedure else flushing with Argon and blank Argon test were repeated. Before each dispersion, traces of air present in the furnace were thoroughly flushed with Argon gas once again creating an inert atmosphere for the pyrolysis phenomenon to take place. Weighed organic powder samples were deposited in the dust chamber/holder and dispersed into the heated chamber at the set temperature. Flash pyrolysis operating conditions and experimental procedures are discussed in Chapter 3.

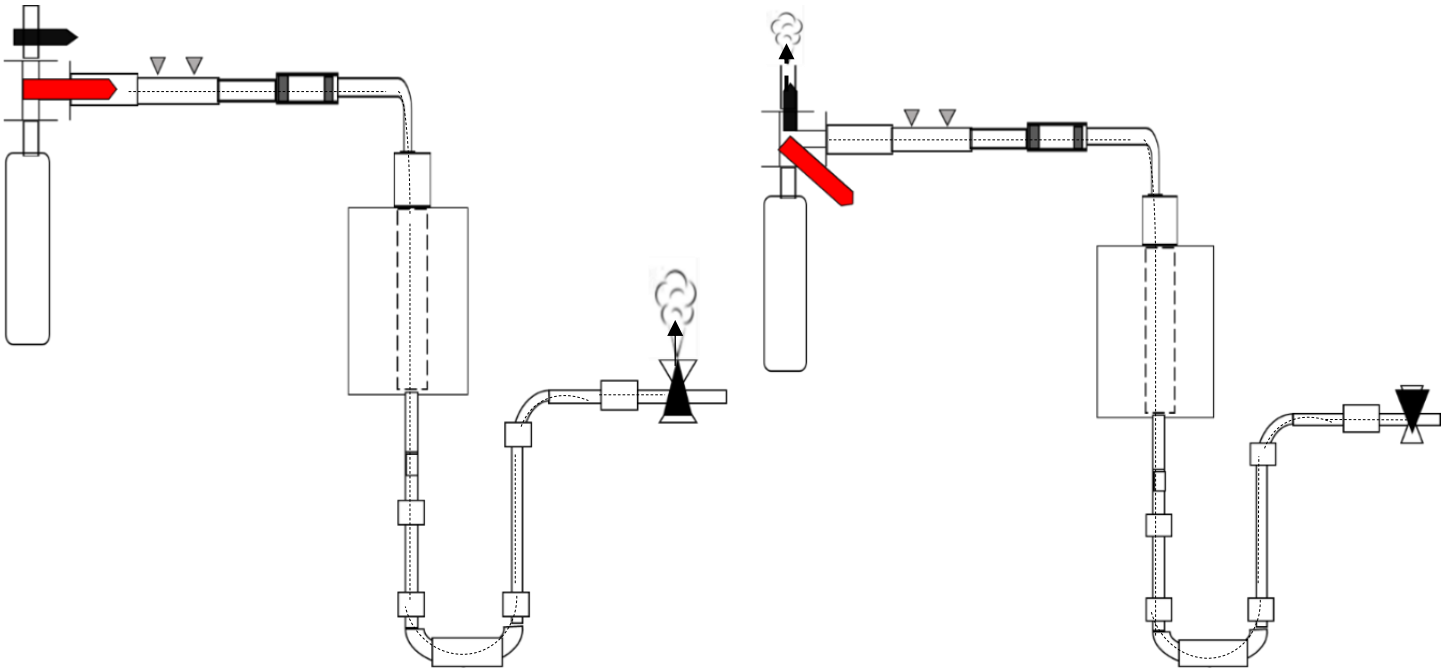

Figure 11: Powder dispersion/flash pyrolysis configuration to the left and Argon Flushing configuration to the right.

3.0 Materials and Experimental Procedure

3.1 Samples

The samples used in this study were microcrystalline cellulose from DuPont (Avicel PH-101), wheat starch purchased from Sigma Aldrich, and oak harvested in Haut-Beaujolais (South-East of France). Cellulose has a linear β-(1→4)-linked glucan structure that gives it a strong hydrogen bond pattern, stiffening its chains resulting in mechanically stable insoluble fibres [23]. Wheat starch on the other hand is linked mainly by branched α-(1→4) glucan structure resulting in a more helical chain configuration with a spherical morphology [66]. To get closer to real scenarios at which powders explode in the process industries two lignocellulosic biomass samples (Oak and Douglas) were used. The abundance of these samples makes it possible to study the varying thermal behaviour of organic dust as a function of its chemical structures, shape, size and form.

3.1.2 Sample Preparation

Oak (hardwood) and Douglas (softwood) samples were initially chunked into small-sized chips excluding the bark followed by knife milling (Retsch SM 300) at 1500 rpm. Perforated screens with hole sizes 10, 5 and 2 mm were used interchangeably in the knife mill to obtain powdered biomass samples. Powdered samples were later sieved for 5 minutes in an AS 200 vibratory shaker (1.01 mm/"g" amplitude) with 315, 180, and 56 µm sieves stacked to each other. Fraction of samples obtained from each sieve size were collected for particle size analysis. Oak and Douglas fir samples less than or equal to 56 µm sieve size were used for flash pyrolysis experiments.

Figure 12: Images of raw (A) Cellulose (B) Wheat starch (C) Oak (D) Douglas fir samples

3.2 Materials Characterisation

3.2.1 Particle size analyses

Particle size analyses were carried out to determine the size distribution of particles present in each sample. The characterisation was also necessary to observe and explain the phenomenon of agglomeration and/or fragmentation during powder dispersion in the Godbert-Greenwald furnace. Helos (Sympatec) Laser Diffraction, Mastersizer 2000 and 3000 (Malvern) instruments were used for the particle size distribution (PSD) in wet and dry powder dispersion measurement modes. Wet or liquid dispersion methods are commonly used in industries to quickly analyse sub-micron particles. The absence of particle-to-particle adhesion forces due to wetting enables particles to be dispersed with relatively lower energy. The method however may not apply to all samples for lack of suitable dispersants. The dry dispersion method on the other hand is suitable for dry powder samples which form agglomerates like in the case of dust explosions.

Particle Size analyses by wet method

The wet analysis allows sample dispersion over a large size range and is the most preferred dispersion approach for sediments, sand and sub-micron clay particles [103]. The Mastersizer 2000 (Malvern) instrument can accurately measure particles over a wide size range from 0.02 µm - 2000 µm for both wet and dry analysis [104]. Particle size distribution of the samples (wheat & starch) for wet analysis were measured with a Malvern Mastersizer 2000 particle size analyser fitted to a Hydro 2000SM dispersion unit. Ethanol was used as the solvent for sample dispersion to avoid swelling in cellulose particles. Approximately 1 g of each sample was added dropwise to about 80 ml of dispersant until an obscuration between 10 % - 20 % was attained. The small volume of the Hydro 2000SM makes it suitable to disperse solvents, expensive and or hazardous samples. With the help of a stirrer operating at 1600 rpm sample particles were agitated and suspended in the ethanol dispersant. The sample/dispersant suspension was delivered to the optical bench for measurements (d_{10}, d_{50}, and d_{90} quantiles of the volumetric distribution).

Due to continuous improvement and equipment upgrade at LRGP, the Malvern Mastersizer 2000 was replaced with a Mastersizer 3000 particle size analyser for Oak and Douglas PSD analysis. The equipment was operated in the dry dispersion mode using 2 bars of pressurised air and a 70 % opening for the funnel in the dispersion unit.

Wetting of particles by dispersant decreases their surface energy and attractive forces [105], which is not the case during sample dispersion in the G—G Furnace. Hence, a dry dust dispersion analysis was carried out.to overcome this limitation,

Particle Size analyses by dry method

Micron, sub-micron and nanosized range particles tend to form agglomerates under very dry conditions due to cohesive forces [106]. To accurately determine the PSD of sample particles and highlight the phenomenon of agglomeration, in-situ dry dust analyses were done with a Sympatec HELOS Laser Diffraction Sensor (Sympatec with a 5mW helium-neon laser source) with the modified Godbert—Greenwald Furnace as the dispersion unit. Particle size measurements were done at the exit of the dust chamber/holder and vertical furnace tube shown by yellow stars in Figure 10. All measurements were conducted thrice to confirm reproducibility.

3.2.2. Image Analyses

Particle morphology of powder samples was studied using a 5 Mp Dino-lite Pro HR digital microscope. Data about particle length and diameter were collected to determine their average shape factors and introduce in the software to take the particle shape into account during PSD measurements.

3.3. Powder Segregation in the Modified Godbert—Greenwald furnace.

Powder segregation in the Modified Godbert-Greenwald furnace was studied to elucidate the quantity of dust that passes through the heated chamber of the furnace after dust dispersion. 1 g of Avicel PH-101 was dispersed in 5 folds of 0.2 g in the furnace with Argon as the carrier gas. Dispersions were carried out at set temperatures from 30 — 300°C. The set-up was allowed to cool down to room temperature and major components of the furnace acting as a pathway for the dusts were taken apart (including the collapsible Tedlar bag for permanent gas collection). The number of settled dust particles on each component were collected and weighed thanks to a Mettler Toledo AE 240 Analytical balance with 0.1 mg readability. At each set temperature, the experimental procedure was repeated thrice for the reason of reproducibility.

3.4 Experimental Procedure

3.4.1 Flash Pyrolysis Step

Flash pyrolysis tests were carried out with the Godbert-Greenwald furnace, which is conventionally used as the standard set-up to determine Minimum Ignition Temperature (MIT) of dust clouds (ISO/IEC 80079-20-2 standard). The method used for powder dispersion in this work is similar to the approach by Dufaud et al [14] as described previously in Chapter 2. Powders present in the dust chamber were dispersed by a pulse of Argon gas at 1.4 bar into the vertical tubular furnace that is electrically heated within the temperature range 700 — 900°C with a step size of 100°C. This temperature range was selected based on proximity to realistic study and representation of dust explosions while considering the maximum temperature limit of the furnace. At each set temperature, 0.2 g of the powder sample was dispersed from the dust chamber into the hot vertical tubular furnace operating at about $1000^{\circ}Cs^{-1}$ heating rate, and dust residence time within the range of 150 — 250 ms determined with a high-speed video camera [107]. Pyrolysis products obtained after each test were collected at the exit of the furnace. Solid residues (char) were collected in the double-layered metallic mesh trap. Condensable gases were cooled into tars in the U-tube shaped section inserted in a Deware vase containing isopropyl alcohol at -30°C. Permanent gas produced was collected in a collapsible Tedlar bag for analysis. To prevent variation of permanent gas composition, only the gas product after first dispersion was collected for analysis. Dispersion of samples was quintupled to reach a mass of 1 g per test due to experimental limitations yielding the minimum amount necessary for solid residue and tar analysis. Experimental procedures were conducted in triplicates for each sample.

3.4.2. Pyrolysis Products Analysis

The thermochemical conversion of the dispersed dust samples in the absence of oxidising agent resulted in the solid residue (char), tar and permanent gas production. The experimental set-up was allowed to cool to room temperature, isopropyl bath taken off and major components of the set-up taken apart to analyse pyrolysis products.

3.4.2.1. Solid Residue

Due to the colour variation after pyrolysis, residues retrieved from the solid trap were subjected to optic microscopy analysis with the 5 Mp Dino-lite Pro HR digital microscope to qualitatively assess their degree of conversion and observe their surface morphology.

To qualitatively assess the solid residues collected at the bottom of the oven, TGA experiments were conducted on the solid residues (cellulose) and later the raw samples in a METTLER TOLEDO **TGA/DSC 1 STA**R^{e} System thermogravimetric analyser. Between 6 and 10 mg of solid residue samples, collected at each pyrolysis temperature were weighed in the thermo-balance and heated from 30° to 950℃ at a heating rate of 15°C/min. All experiments were conducted in a nitrogen atmosphere at a pressure of 1 bar and 50 ml/min flowrate.

3.4.2.2. Tar

Condensable material produced from the flash pyrolysis experiments were analysed with a GC/MS (Agilent 7890A System equipped with a 5975C Triple-Axis detector). Tars in the U-tube shaped section of the experimental set-up (Figure 10) were rinsed with methanol in a 1:3 ratio to enhance its solubilisation. 1 µL of 1-tetradecene was added as an internal standard to the tar/methanol mixture. The resulting solution was filtered through a 0.45 µm polytetrafluoroethylene filter by syringe into vials and about 1 µL was injected into the gas column for analysis. The oven temperature of the GC/MS was programmed from 50°C (5 min) to 250°C at 5°C/min and held constant at 250°C for 10 minutes. The carrier gas used was Helium with a constant flow rate of 24 ml/min, a pressure of 20 psi and a 1:20 split ratio. The T5975C Triple-Axis detector was operated at 300°C with utility (air) and fuel flow of 400 ml/min, 30 ml/min respectively at a data recording rate of 50 Hz. For each identified component, the calculated peak area was converted into a mass yield based on the amount of feed.

3.4.2.3. Gaseous Product

Fast pyrolysis vapours were sampled in a collapsible Tedlar bag and analysed with an SRA 3000 micro gas chromatography fitted to an FID detector. The micro-GC allows identification and quantification of permanent gas (H_2, CO, CO_2, etc), aromatics (toluene, benzene) and hydrocarbon gases (CH_4, C_2H_2, C_2H_4) compositions. Pyrolysis gaseous product was injected into the gas chromatography at a flow rate of 30 ml/min using Helium as the carrier gas at 30 psi pressure. The injector and column temperatures were 100°C and 80°C respectively with a data recording frequency of 50 Hz.

3.4.3. Minimum Ignition Temperature (MIT) Determination

The Minimum Ignition Temperature is the lowest temperature for which hot surfaces will ignite dust clouds. The values normally fall within the range of 150 — 700°C, depending on the nature of materials present in the dust cloud. Materials with low MIT values will have to be handled with care to avoid dust lifting around hot surfaces minimising the risks of explosions [108]. Following the recommendation of ISO/IEC 80079-20-2 standard, MIT tests were conducted in the G—G furnace. Before MIT tests, the condensation chamber of the modified G-G furnace was detached exposing the bottom of the heated chamber to the atmosphere. Two K-thermocouples were placed on the walls of the inner Inconel tube of the heating chamber. Experiments were performed using the guidelines provided by ISO/IEC 80079-20-2. The mode of operation of the G—G-setup is the same as described earlier in Chapter 2 for powder dispersion however, the air was used as the carrier gas. A known mass of powder samples was placed in the dust chamber and dispersed into the heating chamber of the G—G furnace at a set temperature and pressure with pressurised air. A glowing flame was observed at the bottom of the heating chamber to ascertain ignition. Ignition of the samples was assessed based on the following observations:

(a) if a glowing flame was seen, samples were said to have ignited and the corresponding temperature was noted.

(b) the corresponding temperatures of delayed flames were noted and samples were regarded to have ignited.

(c) if a gaseous product was observed with no flame or only smoke, ignition was deemed to have not occurred.

Initially, samples were dispersed at a set temperature while keeping the mass (200 mg) and gas pulse pressure (200 mbar relative to atmosphere) constants during the first part of the test. Temperatures were decreased linearly until the weakest flame was observed. Sensitivity studies were carried out by varying dust masses, and pressures at the lowest furnace wall temperature that could ignite dust clouds. The optimum sample mass, pressure and the corresponding lowest wall temperature/MIT Observed (*Tw*) were recorded. According to ISO/IEC 80079-20-2 standard, the Minimum Ignition Temperature of the dust cloud is the lowest wall temperature at which the ignition of dust cloud could occur decreased by 20℃. The correction formulas are given by equations 1 and 2.

If Tw > 300℃ *; Tc=Tw* - 20℃ (1)

If Tw ≤ *300*℃ *; Tc=Tw* - 10℃ (2)

Dust clouds were dispersed 10 times at the corrected Ignition temperature (Tc) to confirm no ignition occurred. The GG-set up was calibrated with lycopodium powder before sample dispersion and ignition. Cellulose, wheat starch and oak (56—180 μm) samples were used for MIT tests.

4.0 RESULTS AND DISCUSSION

4.1 Sample Characterisation

4.1.1 Particle size analysis

Results for particle size analysis (wheat starch and cellulose) done by wet way method using the master sizer 2000 is illustrated in Figure 13. Wheat starch samples showed a bimodal distribution with particle size centred at 3 and 30 μm. Cellulose particles on the other hand demonstrated a unimodal distribution with the majority of particles distributed around 90 μm**.** Particle size analysis of the lignocellulosic biomasses (oak and douglas) were carried out in a dry way dispersion using the master sizer 3000. Results obtained are also presented in Figure 13 Oak and douglas fir powders showed mono-modal distribution with the majority of particles cantered around 55 μm. Table 5 presents the D_{10}, D_{50} and D_{90} parameters for all dust samples used during experiments.

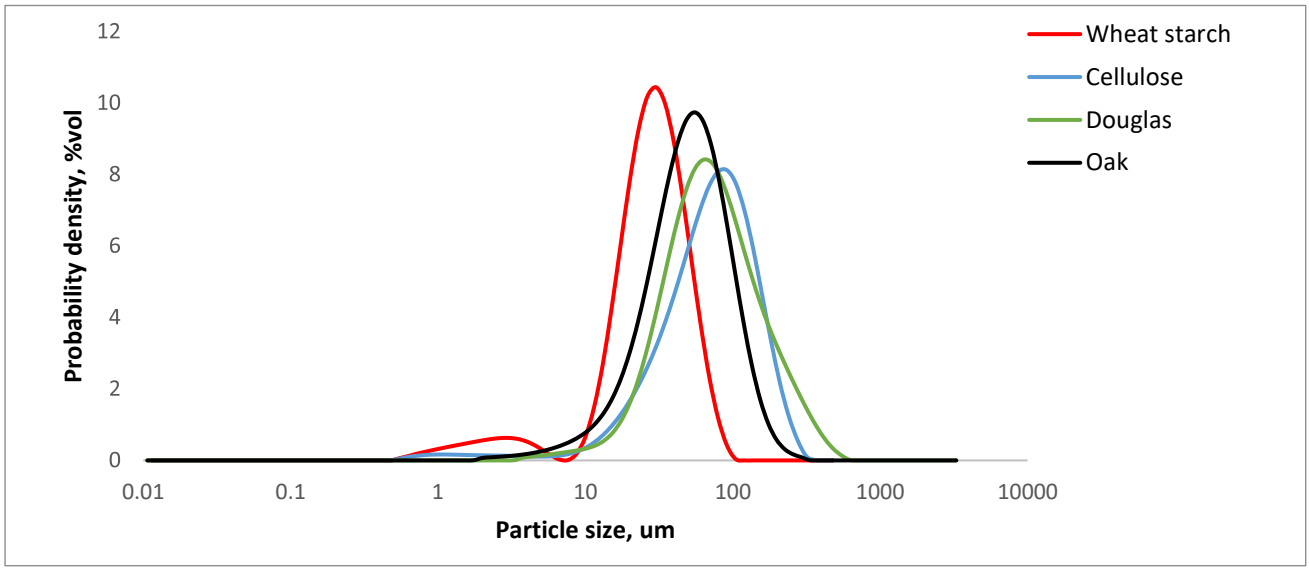

Figure 13: Particle size distribution for cellulose, wheat starch, oak and douglas fir samples.

Table 5: D_{10}, D_{50} and D_{90} characteristic parameters for organic powder samples

Samples	D_{10}	D_{50}	D_{90}
Wheat Starch	11.8	26.4	49.5
Cellulose	22.2	67.9	146.1
Oak	19.6	50.5	107
Douglas	18.7	47.8	86.2

Figures 14 and 15 show the PSD analysis for cellulose and wheat starch dust clouds before (end of the dust holder) and after the heated chamber (exit of the furnace). Particle-to-particle interaction during dust dispersion was negligible at the entrance to the furnace but pronounced in the furnace giving rise to particles within the 350 μm size range. The particle size increase at the furnace exit can be attributed to powder agglomeration during dust dispersion. A similar trend was observed in both cellulose and starch dust clouds.

4.1.2 Optic Analysis

Optic microscopy was used to study the different morphologies of the samples as illustrated in Figure 16. Cellulose microfibrils exhibited elongated shape but more spherical particles were observed for

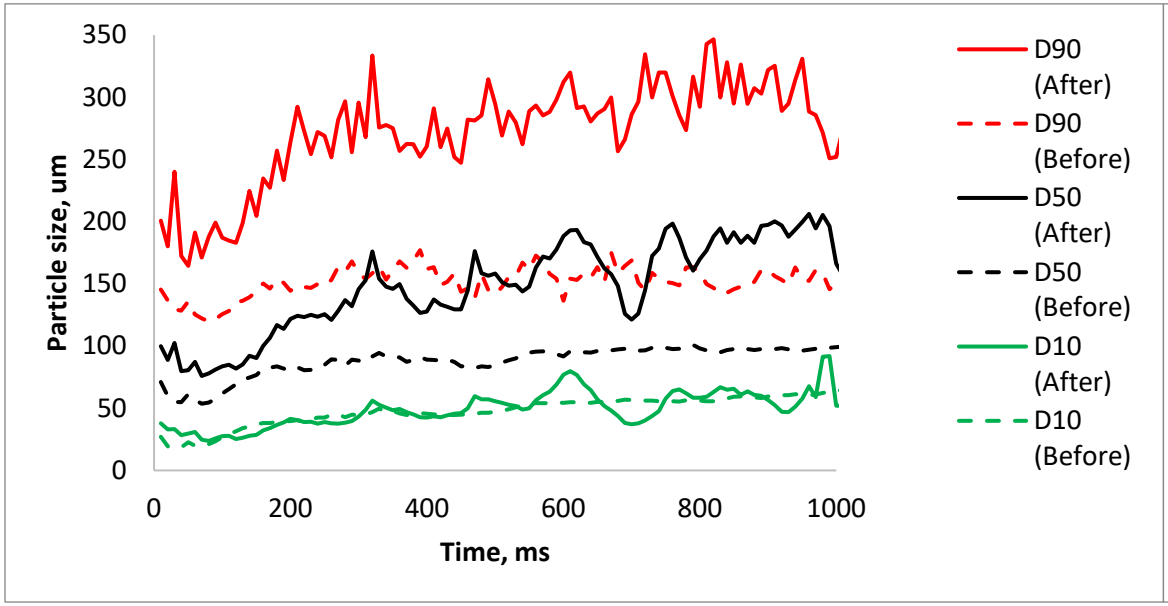

Figure 15: D_{10}, D_{50}, and D_{90} Characteristics parameters of dispersed cellulose dust before and the heated furnace as a function of time

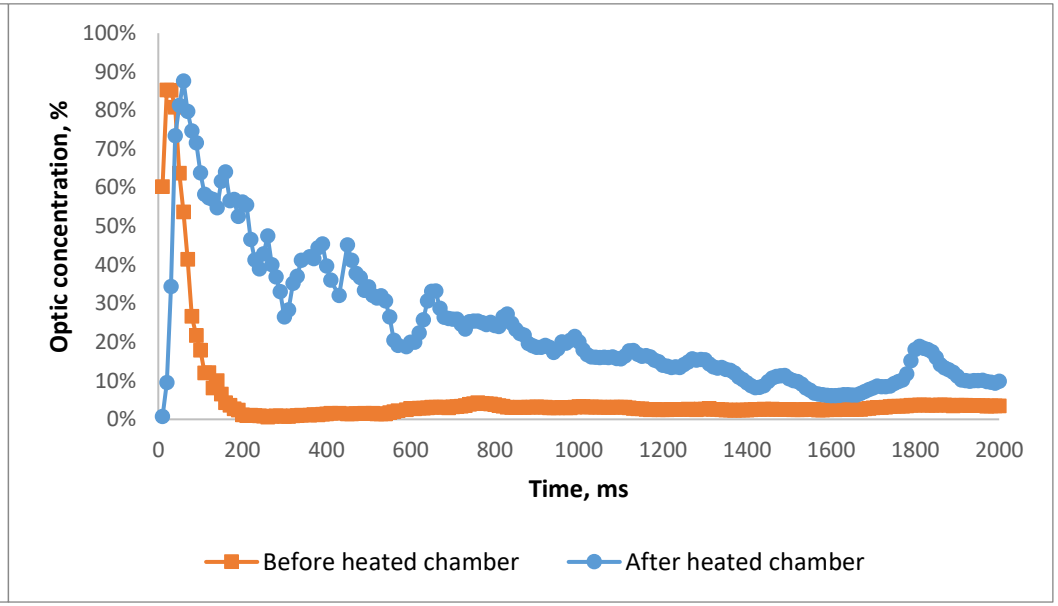

Figure 14: Optic concentration of dispersed wheat starch cloud before and after the heated chamber as a function of time

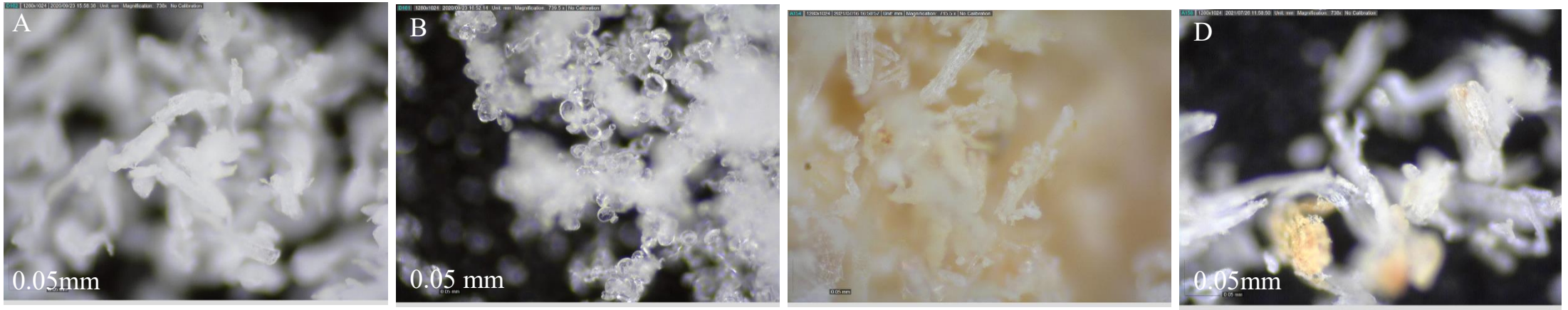

Figure 16: Optical imaging of raw starch (A) cellulose (B) wheat starch (C) oak (D) dougals fir sample

starch samples. Lignocellulosic samples (oak and douglas) also showed elongated fibrous structures. A light red fibrous structure was seen in the oak samples indicating lignified cells such as sclereids, xylem or phloem fibres [109].

4.2. Apparatus Characterisation

Figure 17 gives a representation of the quantity of dispersed powder that passed through the G-G set-up during the experimental procedure. The powder segregation is done on the setup revealed majority (at least 70 %) of the dispersed powder moved through the heated chamber. Remnants of powder in the upper parts of the set up (purge gas outlet, dust chamber, rubber and elbow joint combined) during dispersion were negligible (0.13 ±0.02 % – 1.2± 0.2 %). A small amount of undispersed powder was found on top of the vertical tube (2.7 ± 1% – 6.9 ±1 %). This necessitates slight modifications to the setup to maximise the overall amount of dispersed dust. At room temperature (30℃) approximately 82±4 % of the dispersed cellulose dust moved through the heated chamber of the furnace whereas close to 5±3 % of the cellulose powders adhered to the walls of the vertical tube in the heated chamber. Before powder segregation, the moisture content of the Avicel PH 101 determined after oven drying for 12 hours was 4 %. This had a direct influence on powder flowability, which decreases with increasing moisture content [110]. The low flowability at room temperature in Avicel PH 101 explains why appreciable amounts of powders adhered to the vertical tube walls during dispersion. At 100℃ dehydration begun in the cellulose, decreasing the moisture content while increasing flowability as a result 89 ±6 % of the dust passed through the furnace [61], [110]. Dust dispersion at 200℃ showed a similar trend observed at 100℃ however, only 82 ±9 % of the dust was observed to have passed through the furnace. The maximum amount of undispersed powder at the top of the vertical tube (6.9±1 %) was collected at this temperature (200℃). As dispersion temperature rose the number of powders which adhered to the vertical tube walls decreased: 1.1±0.9 % at 100℃, 0.4 ±0.2 % at 200℃ and 1.4±0.3 % at 300℃. The amount of powder that moved through the heated chamber was slightly low (68.14±4 %) at 300℃ due to the onset of pyrolysis, fractions of the dispersed dust were already being converted into pyrolytic products [61]. The slightly brown colouration of the collected powder sample confirmed pyrolysis onset at 300℃. Calculations for the mass yield of powder segregations are shown in Annexe 1. Based on the results obtained, semi-quantitative calculations of pyrolysis conversions could be estimated.

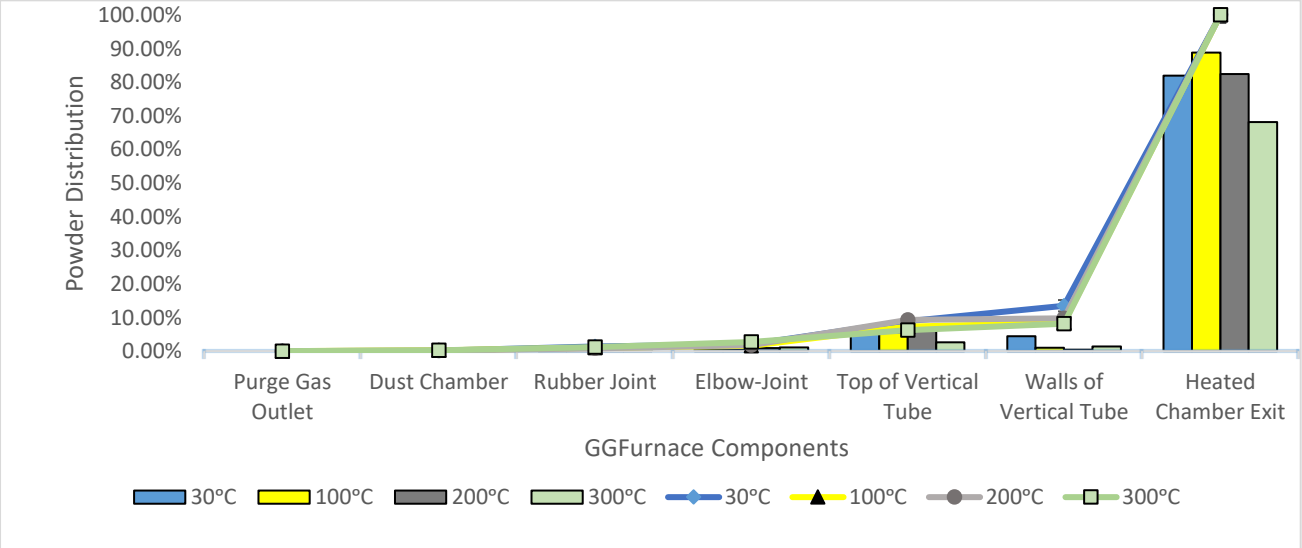

Figure 17: Organic dust segregation in the G—G furnace during dispersion

4.3. Flash Pyrolysis Step

4.3.1 Optic Imaging of Solid Residues

Image analysis of solid residues collected from the solid trap is shown in Figure 18 for cellulose, wheat starch, oak and douglas fir samples. Imaging results observed is a mixture of white, dark brown and black colouration patches on the residues. The colour variation indicates incomplete pyrolysis primarily due to dust samples inability to reach reactor temperatures. The white colouration observed in some parts of cellulose and wheat starch solid residues indicates that the activation energy required for pyrolysis reaction to occur was not attained in all samples due to inhomogeneous heat transfer in the dispersed dust. A similar trend was seen in oak and douglas fir samples where some parts of the initial light brown colouration which was previously observed in the raw samples remained unchanged. The extremely short feed residence time (between 150 and 250 ms) is an added reason for the incomplete solid residue conversion. On the other hand, solid residue conversion increased with temperature as residues close to char were observed at elevated reactor temperatures.

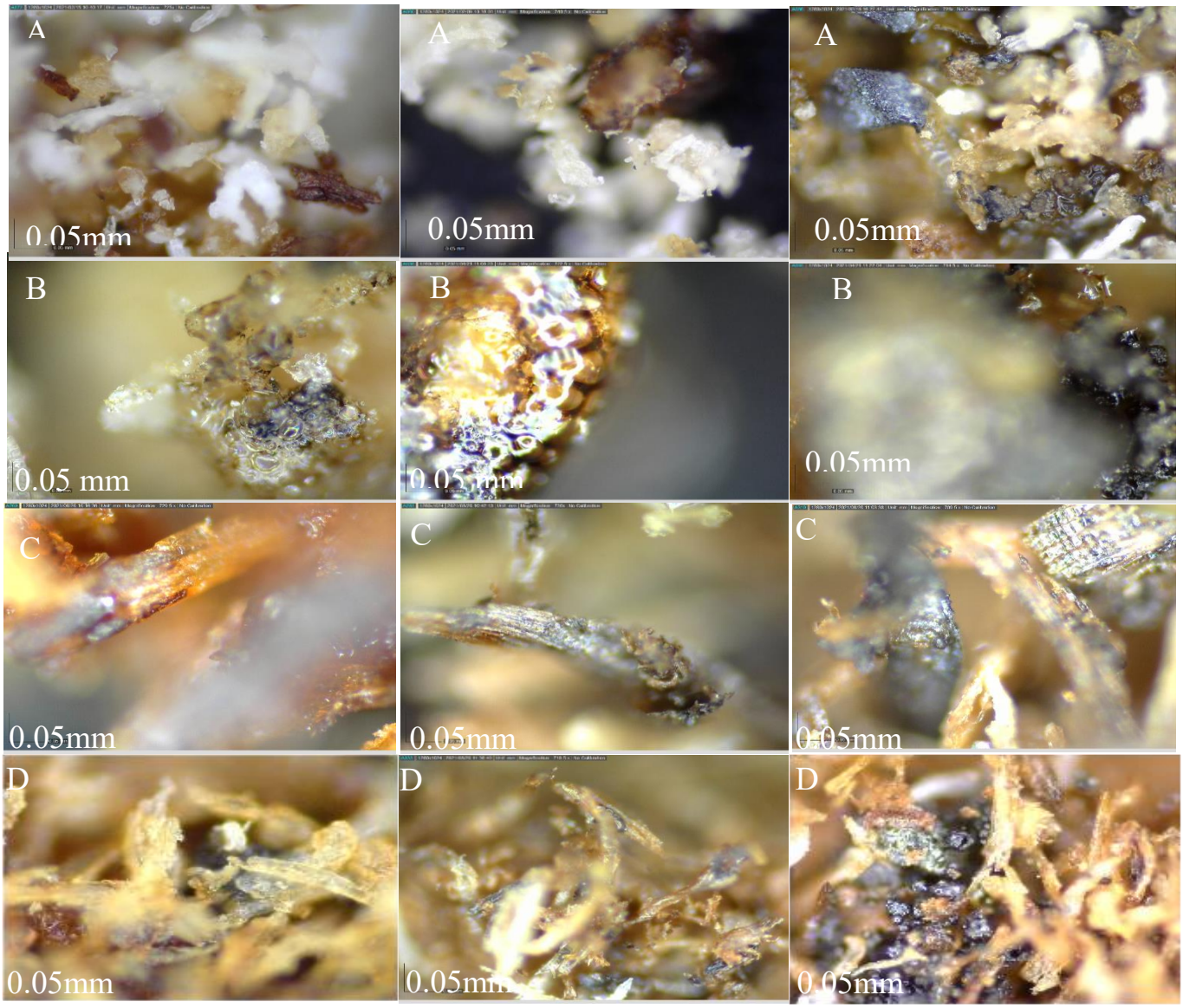

Figure 18: Solid residues images for (A) cellulose (B) wheat starch (C) Oak, (D) Douglas at 700, 800 and 900°C from left to right.

4.3.2 TG ANALYSIS

The thermal behaviour of raw cellulose, oak and douglas samples were studied alongside the solid residues of cellulose retrieved from the solid trap of the G—G setup. Figure 19 represents the weight loss for the various samples in the TGA.

The decomposition temperature range of cellulose samples was narrow as expected [77]. An initial mass loss of around 120°C is attributed to dehydration in the cellulose samples. This is followed by the onset of decomposition around 280°C and a rapid devolatilization until a maximum decomposition rate occurs at approximately 340°C.

For the lignocellulosic biomass samples (oak and douglas fir) the TG-DTG thermograms represent mass loss by water and extractives followed by decomposition of hemicellulose, cellulose and lignin components.

Lignocellulosic biomass (oak and douglas) components presented in Table 6 were reported in another work [98]. In the thermograms for oak shown in Figure 19, two extensive peaks were observed. The first peak was seen in the temperature ranges of 250°C — 350°C and then a second peak within the temperature ranges of 350°C — 400°C [84]. The first peak accounts for hemicellulose decomposition with a maximum degradation rate occurring at 317°C. The second peak on the other hand was mainly due to cellulose decomposition with a corresponding maximum degradation rate occurring at 380°C, which is higher than that of raw cellulose. The difference in the maximum degradation rate for raw cellulose and cellulose component in oak samples could be attributed to component interaction within oak as previously discussed in Chapter 1.2.6.4. A slower mass loss was observed for lignin beyond 500°C. From the TGA analysis, thermal behaviour was similar in both lignocellulosic biomasses (oak and douglas fir) however, the two extensive peaks observed earlier were less pronounced in douglas fir. This can be attributed to lower cellulose and hemicellulose content in raw douglas samples compared to oak as shown in Table 6. The lignin content on the other hand is slightly higher in douglas fir contributing to a slightly higher thermal decomposition temperature as suggested earlier in the literature review by Greenhalf et al [97]. The maximum decomposition rate occurred around 350°C, and 390°C for hemicellulose and cellulose respectively in douglas fir. Based on the TGA analysis, organic dust was thermally decomposed approximately at 340°C for cellulose and 400°C for both lignocellulosic biomasses (oak and douglas fir) followed by a subsequent release of volatiles (Gaseous products) which propagates together with a flame in a confined space causing an explosion. A schematic representation of the suggested explosion pathway is shown in Figure 20.

It is interesting to note, some amount of dispersed dust remains at the bottom of the Inconel tube attached to the Heated Chamber exit as such residues collected in the solid trap is not a global representation for all residues. This, coupled with the low solid residue conversion into char confirmed by microscopic images in chapter 4.3.1 makes it very difficult to perform a mass balance of pyrolytic products in the G—G setup.

Table 6: Lignocellulosic biomass composition adapted from [54]

	Lignocellulosic Biomass	
Properties	Oak	Douglas fir
Lignin (% db)	24.2	34.4
Cellulose (% daf)	51	44
Hemicellulos (% daf)	34	29

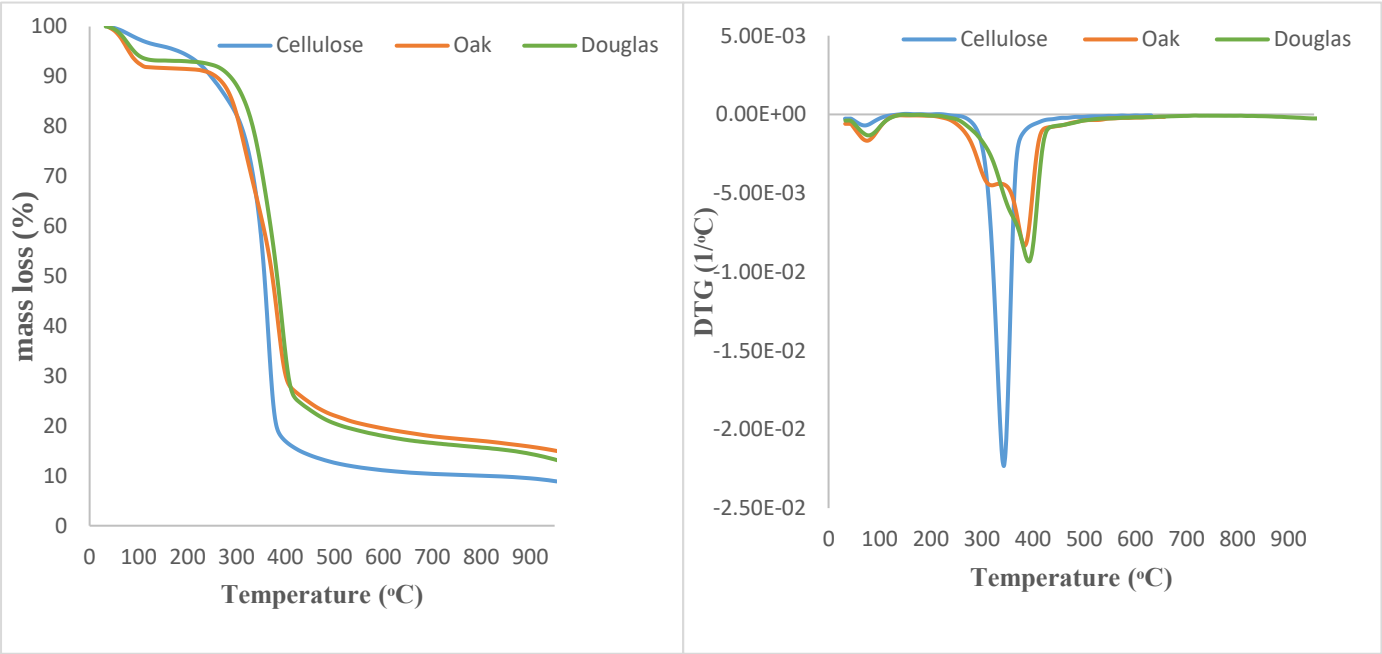

Figure 19: TG (left) and dTG (right) thermogram of cellulose, oak and douglas fir samples.

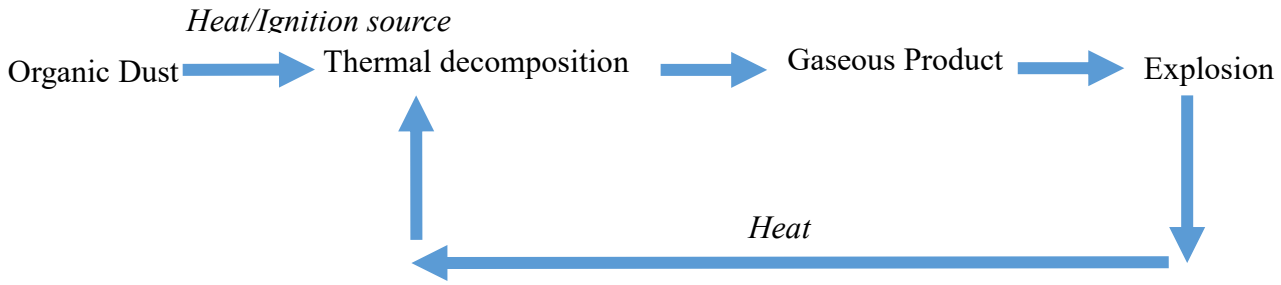

Figure 20: Schematic representation of the pathway of organic dust explosion adapted from [111].

Cellulose solid residues collected from the solid trap at various temperatures in the G-G set-up were altered slightly. Their onset of decomposition was approximately at 317°C, 315°C and 319°C with corresponding maximum decomposition rates occurring at 366°C, 370°C and 375°C for residues retrieved at 700°C, 800°C and 900°C respectively. The TG-DTG curves in Figure 19 generally represent weight loss by dehydration (120°C) followed by solid residue degradation. Residual volatile matter content estimated from the thermograms were approximately 87, 89 and 83% respectively for solid residues retrieved at 700, 800 and 900°C. That is, the residual volatile matter contents in the solid residues generally decreased with increasing reactor temperature. These estimated values are relatively high compared to torrefied wood with a residual volatile matter of around 64% [112]. This confirms only partial pyrolysis of biomass samples in the G-G setup already mentioned in Chapter 4.3.1. The TG-DTG curves for cellulose solid residues are shown in Figure 21.

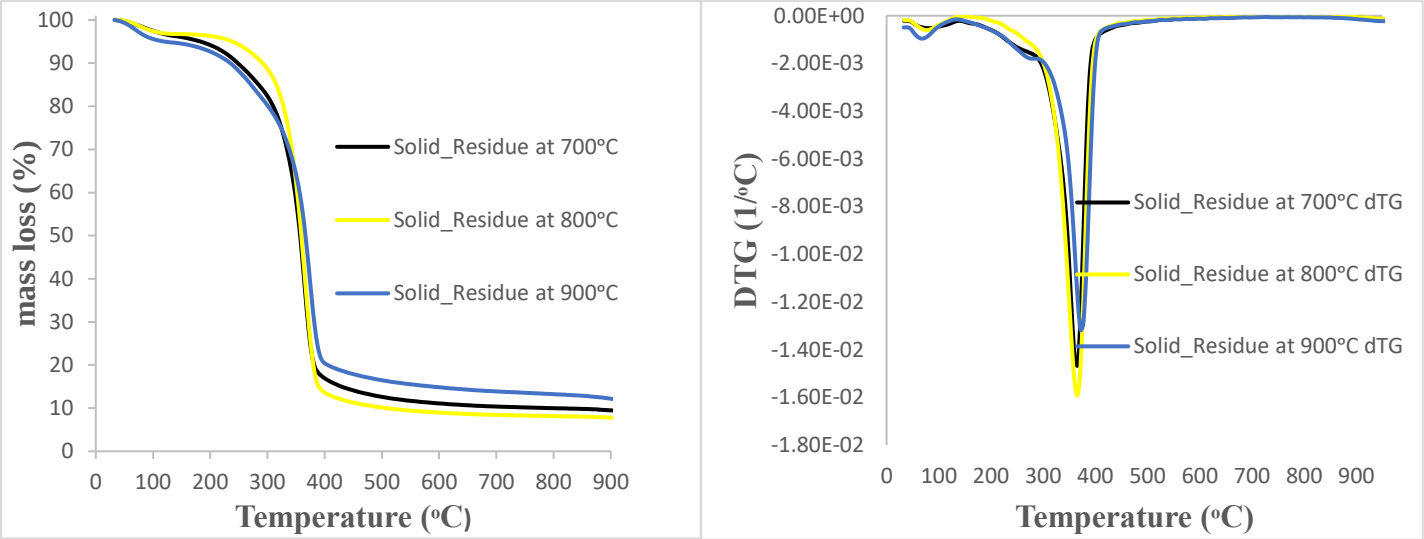

Figure 21: TG (left) and dTG (right) thermogram of cellulose solid residues

4.3.3 Tar analysis

Tar compositions produced during flash pyrolysis experiments were analysed by GC/MS-FID. Due to the relatively low tar yield, only components with prominent peak areas were considered in this work notwithstanding the numerous tar constituents [23]. A relative response factor (RRF) of 4.47 between levoglucosan and 1-tetradecene that had been already determined was used to analyse mass yields based on raw data from the GC/MS. Yields of some well-known products (levoglucosan) were influenced by the reactor temperature [23][65]. Results of major components present in the tars after cellulose decomposition are presented in Table 7. The results obtained are in agreement with the literature that levoglucosan is the main tar constituent of cellulose pyrolysis [33][65]. Increasing the reactor temperature seemed to have favoured the Levoglucosan yield due to their thermal stability as demonstrated by Lu et al [33], with the maximum yield occurring at a reactor temperature of 800°C. Levoglucosan was formed by the splitting of (1,4) glycosidic bonds in cellulose powders followed by monomer units rearrangement [113]. Small yields of oxygenated compounds (hydroxyacetone, dihydroxyacetone, cyclopentanepentol) and alkane (2-2-dimethoxybutane) were also detected. It is interesting to note that the poor thermal conductivity of cellulose contributes to its lower pyrolysis reaction temperature[114], however, the significantly low tar constituents (particularly levoglucosan) yield obtained in this work compared to literature [115] is an indication of partial pyrolysis.

Table 7: Tar compositions and yield after cellulose pyrolysis at varying reactor temperatures.

Parameters			Product Yield (wt %) at reactor temperature (700°C)	Product Yield (wt %) at reactor temperature (800°C)	Product Yield (wt %) at reactor temperature (900°C)	Levoglucosan yield (wt %) at 850°C	Levoglucosan yield (wt %) at 1000°C
Retention time (min)	Compound Name	Chemical Formula					
5.134	hydroxyacetone	$C_3H_6O_2$	n.d	n.d	0.030		
7.973	dihydroxyacetone	$C_3H_6O_3$	0.035	0.047	0.029		
8.812	2-2-dimethoxybutane	$C_6H_{14}O_2$	0.003	n.d	n.d	—	—
17.927	2,6,7-trimethyldecane	$C_{13}H_{22}$	0.002	n.d	n.d		
28.901	1,2,3,4,5-cyclopentanepentol	$C_5H_{10}O_5$	n.d	n.d	0.003		
34.124	Levoglucosan	$C_6H_{10}O_5$	0.516	0.91	0.662	*5.2	*7.5

n.d = not detected
Yield in wt % is based on the mass of organic powder
* Levoglucosan yield of Avicel PH 102 obtained from a bench-scale tubular reactor (Length: 30 cm) [115].

Tar constituents from wheat starch pyrolysis varied slightly from cellulose tar compositions, both sugars derived components (Levoglucosan) and oxygenated compounds (hydroxyacetaldehyde) were identified as major components. The α (1→4) glycosidic bonds were cleaved during wheat starch pyrolysis resulting in the formation of free glycosidic radicals that directly transformed into levoglucosan. The remaining glycosidic bonds were converted into volatiles (dominated by hydroxyacetaldehyde) and solid residues [72]. Results for wheat starch tar composition are presented in Table 8. All calculations for cellulose and wheat starch tar composition and yield are attached in Annexe 2.

Table 8: Tar composition of wheat starch pyrolysis at varying reactor temperatures.

Parameters			Product Yield (wt %) at reactor temperature (700°C)	Product Yield (wt %) at reactor temperature (800°C)	Product Yield (wt %) at reactor temperature (900°C)	Levoglucosan yield (wt %) At 420°C
Retention Time (min)	Compound Name	Chemical Formula				
5.42	Hydroxyacetaldehyde	$C_2H_4O_3$	0.021	n.d	0.074	
	Glyoxylic acid methyl ester	$C_3H_4O_4$	0.007	n.d	0.005	
7.972	Dihydroxyacetone	$C_3H_6O_3$	n.d	0.032	0.011	—
	Glycoaldehyde dimer	$C_4H_8O_5$	n.d	0.042	n.d	
34.294	Levoglucosan	$C_6H_{10}O_6$	n.d	0.09	0.02	14**
	Ethanol, 1 methoxy-benzonate	$C_{10}H_{12}O_4$	0.003	n.d	n.d	

** Levoglucosan yield of corn starch pyrolysis under N_2 atmosphere in a downflow concurrent tubular furnace reactor (Length: 54 cm) with residence times between 35 – 75 ms [72].

4.3.4 Gaseous Products

Figure 22 illustrates the composition and yields of gaseous products for all samples analysed with the micro—GC. The major gaseous components identified were H_2, CO, CH_4 and CO_2 as they account for more than 86 % of the dry gas composition. H_2, CO, and CH_4 increase with increasing reactor temperature while CO_2 shows the opposite trend [36], [44]–[46]. This trend in CO_2 can be explained by two main reasons;

(i) carboxyl groups which decompose to release CO_2 degrade at lower temperatures resulting in low CO_2 yield at higher reactor temperature [36]

(ii) at higher reactor temperature secondary reactions such as the Boudouard reaction (3), gasification reaction (4), and reverse water gas shift reaction (5) are likely to occur causing CO_2 reforming to H_2 and CO [116].

Boudouard reaction	$C + CO_2 \rightleftharpoons 2CO$	(3)
Gasification reaction	$C + H_2O \rightleftharpoons CO + H_2$	(4)
Reverse water gas shift reaction	$CO_2 + H_2 \rightleftharpoons CO + H_2O$	(5)

The principal components of pyrolysis gas (H_2 and CO) generally increased with reactor temperature reaching maximum yields of 70.13, 74.9, 58.67 and 73.45 mol % for cellulose, wheat starch, oak and douglas fir respectively which are in good agreement with literature. In the work of Wei et al [36], a maximum H_2+CO yield of 72.4 and 71.8 mol % was attained for legume straw and sawdust lignocellulosic biomasses at 800°C. Small yields of C_2H_4 (ethylene), C_2H_2 (acetylene) were identified with C_2H_4 (ethylene) showing a slight increase at higher reactor temperature while C_2H_2 (acetylene) decreased minimally as the temperature rose. C_6H_6 (Benzene) was significantly low but showed a similar trend as C_2H_4 (ethylene). The effect of CO_2 reforming to H_2 and CO at elevated temperatures

can be seen in the H_2/CO and CO/CO_2 molar ratios. The H_2/CO ratio exhibited a linear increase but experienced a slight reduction at 900°C for wheat starch, oak and douglas fir while CO/CO_2 ratio increased exponentially due to the higher yields of CO at elevated reactor temperature. This trend is depicted in Figure 23. The CO_2 ratio was unexpectedly high in douglas fir at 900°C resulting in lower H_2/CO and CO/CO_2 ratios than anticipated. The discrepancy can be attributed to air introduction in the G—G furnace causing oxidation reaction to set in. The hydrogen-rich gas produced during the pyrolysis stage of organic dust explosion is at the centre of the phenomenon as they ignite causing flame propagation.

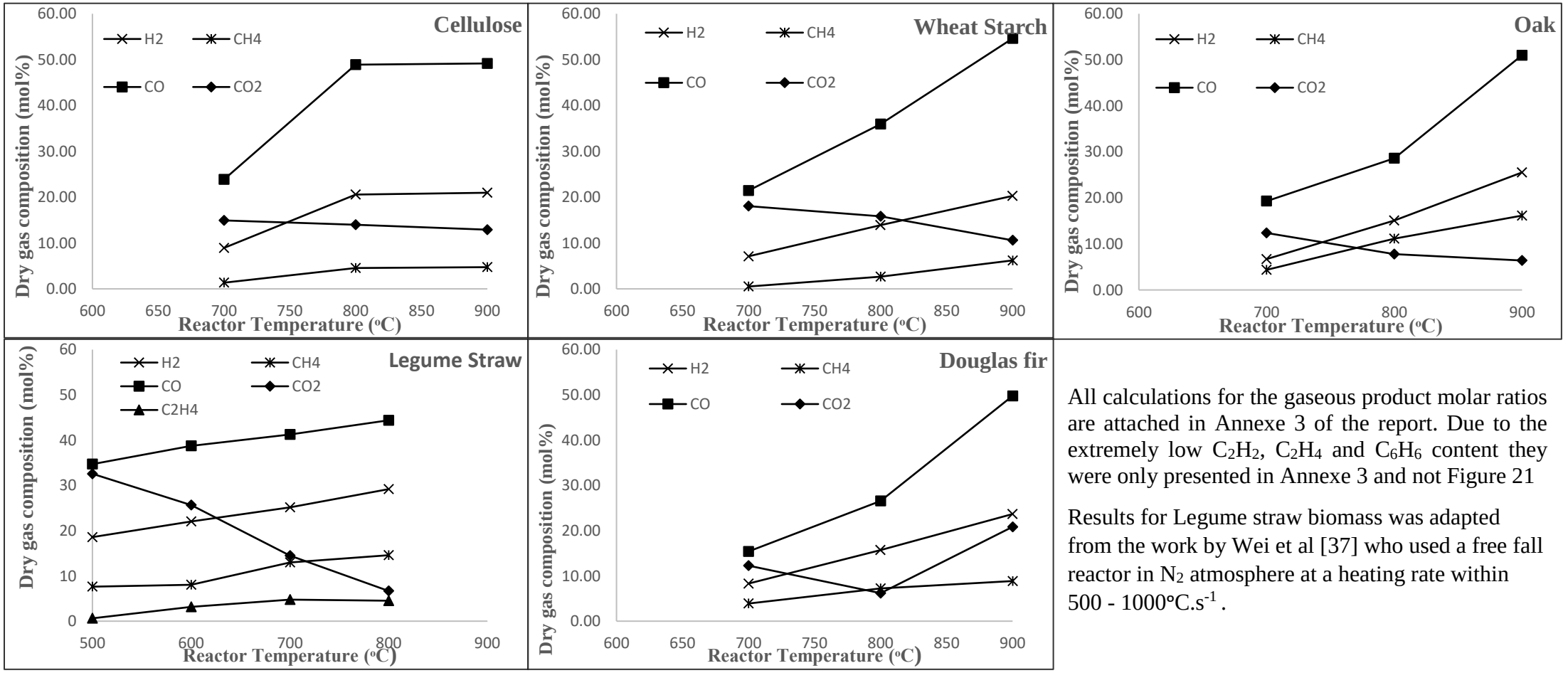

All calculations for the gaseous product molar ratios are attached in Annexe 3 of the report. Due to the extremely low C_2H_2, C_2H_4 and C_6H_6 content they were only presented in Annexe 3 and not Figure 21

Results for Legume straw biomass was adapted from the work by Wei et al [37] who used a free fall reactor in N_2 atmosphere at a heating rate within 500 - 1000°C.s^{-1} .

Figure 22: Effect of reactor temperature on dry gas compositions

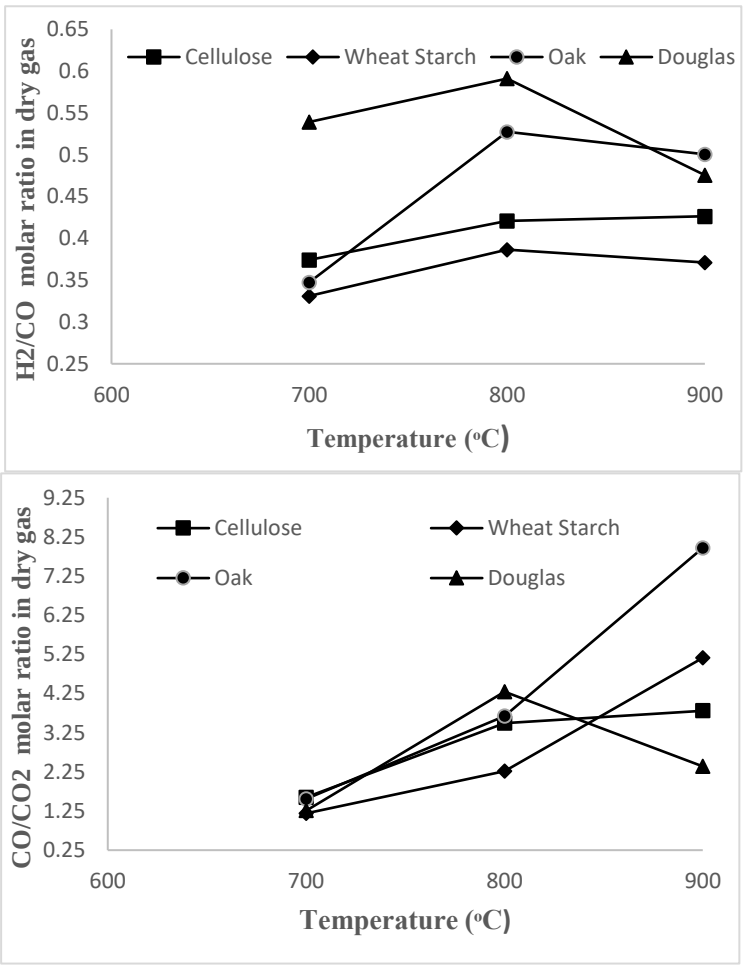

Figure 23: Effect of reactor temperature on H_2/CO, CO/CO_2 molar ratios on dry gas compositions.

4.3.5 Minimum Ignition Temperature

The minimum ignition temperature (MIT) is an essential parameter for assessing dust sensitivity and explosion. It helps to predict ignition caused by hot surfaces such as ovens, friction-induced heated moving parts, etc in process industries that make use of combustible dust [102][117]. MIT results were obtained at maximum dust loading and pressure of 0.3 mg and 0.3 bar (relative to atmosphere) respectively for all samples. Based on this work, hot surfaces with estimated temperatures around 440, 430, and 470°C are most likely to act as an ignition source for cellulose, wheat starch and oak dust. If these combustible organic dusts are dispersed in air within confined areas, the risk of explosion is extremely high. Results for the MIT summarised in Table 9 are in good agreement with literature.

Table 9: Minimum Ignition Temperature for cellulose, wheat starch and oak dust cloud.

Organic Dust	Particle size (d_{50}) μm	MIT of dust cloud (°C)	Reference
Cellulose	68	440	Present Work
	50	410	[117]
Wheat Starch	26	430	Present Work
	35	400	[117]
Oak	167	470	Present Work
	500	500	[118]

5.0 CONCLUSION

This work aimed to study the pyrolysis mechanism for organic dust explosion as pyrolysis can be the rate-controlling step. Organic dust explosion, however, takes place at very high temperatures (1000°C), high heating rate (1000°C.s^{-1}) and extremely short vapour residence time (20 – 50 ms) as such the study of flash pyrolysis mechanism became the focus of this work since it represents realistic proximity to an organic dust explosion.

Firstly, particle size distribution and microscopic imaging analysis were carried out on organic powders (cellulose, wheat starch, oak and douglas fir) to characterize them. It was observed that:

- Wheat starch particles had spherical geometries while cellulose powders showed elongated fibrous shape.
- A similar elongated fibrous structure was observed in both lignocellulosic biomasses (oak and douglas fir).
- The powder agglomeration phenomenon occurs for dust dispersion during the explosion.

Flash pyrolysis experiments were carried out in the G—G furnace capable of reaching extremely fast heating rates (1000°C.s^{-1}) at different reactor temperatures (700 — 900°C). Pyrolysis products obtained for each sample were analysed. Microscopic images of solid residues retrieved from the solid trap of the G—G setup showed patches of colour variation white, light brown and black indicating partial pyrolysis of dispersed dust. TGA results of cellulose solid residue collected at different reactor temperatures (700, 800 and 900°C) confirmed partial pyrolysis of dispersed dust as the residual volatile matter content were still high although it decreased with increasing reactor temperature. TGA of cellulose, wheat starch, oak and douglas fir samples indicated degradation onset temperatures at which the devolatilization of organic dust commence.

GC/MS analysis of the tar condensates for both cellulose and wheat starch were presented. The results showed;

- Levoglucosan was the major product produced during flash pyrolysis of cellulose dust with a maximum yield occurring at a reactor temperature of 800°C. Other oxygenated compounds (hydroxyacetone, dihydroxyacetone, cyclopentanepentol) and alkane (2-2-dimethoxybutane) were also identified but in extremely lower yields.
- Levoglucosan and hydroxyacetaldehyde were the major products for wheat starch pyrolysis. While levoglucosan peaked at 800°C, hydroxyacetaldehyde on the other hand increased with increasing reactor temperature. Levoglucosan yield was lower in cellulose than in wheat starch.

Results for the gaseous pyrolytic products for cellulose, wheat starch, oak and douglas fir were also presented. The effect of reactor temperatures on the gas compositions was studied. H_2 (Hydrogen), CO (Carbon mono-oxide), CO_2 (carbon dioxide) and CH_4 (methane) were identified as major gaseous components alongside small yields of C_2H_2 (acetylene), C_2H_4 (ethylene) and traces of C_6H_6 (benzene). H_2, CO, and CH_4 yields increased with increasing reactor temperature while CO_2 showed an opposite trend due to secondary reactions at elevated temperatures. Such gaseous products have fairly good heating value (17 — 19.5 MJ/kg) which contribute to explosion severity during organic dust explosion.

Finally, the last part of this study focused on the minimum hot surface temperature that could be a potential ignition source for cellulose, wheat starch, and oak dispersed dust clouds. Results indicate dust explosion is likely to occur if cellulose, wheat starch and oak powders are dispersed over a hot surface at 440, 430 and 470°C respectively in the presence of air within a confined area.

5.1. PERSPECTIVES AND RECOMMENDATION

Considering the low degree of solid residues conversion, organic dust residence time seems to be too short for complete pyrolysis to occur. Adjusting the height of the heated chamber could extend dispersed powder residence time and enhance the complete pyrolysis of dust. This will also minimise the probability of dust clogging at the furnace exit, as this was the case for oak and douglas powder dispersion. Due to dust clogging at the furnace exit, tar condensates could not be retrieved and analysed for both oak and douglas fir samples. Identifying the tar compositions and qualitatively assessing solid residues for oak and douglas samples can be done in subsequent work. Using the permanent gas composition in this work, and results that will be obtained from tar and solid residue analysis on oak and douglas samples, a predictive model can be built to determine the pyrolysis rate of reaction for lignocellulosic dust in the G–G setup.

Preheating the carrier gas (Argon) used for flash pyrolysis experiments is another option to consider as it may enhance convective heat transfer for much better pyrolysis reaction and enhance solid residues degree of conversion. The suggestions made can be considered in subsequent work.

REFERENCES

[1] M. Weber, “Some Safety Aspects on the Design of Sparger Systems” *Process Saf. Prog.*, vol. 25, no. 4, pp. 326–330, 2006.

[2] T. Skjold and R. K. Eckhoff, “Dust explosions in the process industries: Research in the twenty-first century,” *Chem. Eng. Trans.*, vol. 48, pp. 337–342, 2016.

[3] Z. Yuan, N. Khakzad, F. Khan, and P. Amyotte, “Dust explosions: A threat to the process industries,” *Process Saf. Environ. Prot.*, vol. 98, pp. 57–71, 2015.

[4] P. R. Amyotte, “Some myths and realities about dust explosions,” *Process Saf. Environ. Prot.*, vol. 92, no. 4, pp. 292–299, 2014.

[5] “Preventing Grain Dust Explosions Starts With You.”.

[6] “The world’s worst coal mining disasters.” [Online]. Available: https://www.mining-technology.com/features/feature-world-worst-coal-mining-disasters-china/. [Accessed: 12-Aug-2021].

[7] M. Weber, “Imperial Sugar Refinery Combustible Dust Explosion Investigation,” *Process Saf. Prog.*, vol. 25, no. 4, pp. 326–330, 2006.

[8] R. K. Eckhoff, “Current status and expected future trends in dust explosion research,” *J. Loss Prev. Process Ind.*, vol. 18, no. 4–6, pp. 225–237, 2005.

[9] P. Pico, N. Ratkovich, F. Muñoz, and O. Dufaud, “Analysis of the explosion behaviour of wheat starch/pyrolysis gases hybrid mixtures through experimentation and CFD-DPM simulations,” *Powder Technol.*, vol. 374, pp. 330–347, 2020.

[10] A. Santandrea, “PhD title from the University of Lorraine In-Process and Product Engineering and Molecules by Chemical Engineer - ENSIC New insights on the explosion severity of nanopowders : a nano-grain of sand in the gears of the standards.”

[11] D. Torrado *et al.*, “Explosions of gas/carbon black nanoparticles mixtures: An approach to assess the role of soot formation,” *Chem. Eng. Trans.*, vol. 48, pp. 379–384, 2016.

[12] S. Callé, L. Klaba, D. Thomas, L. Perrin, and O. Dufaud, “Influence of the size distribution and concentration on wood dust explosion: Experiments and reaction modelling,” *Powder Technol.*, vol. 157, no. 1–3, pp. 144–148, 2005.

[13] M. Pietraccini *et al.*, “Determination of heterogeneous reaction mechanisms: A key milestone in dust explosion modelling,” *J. Loss Prev. Process Ind.*, vol. 73, p. 104589, Nov. 2021.

[14] O. Dufaud *et al.*, “Comparing pyrolysis gases and dusts explosivities: A clue to understanding hybrid mixtures explosions?,” *Ind. Eng. Chem. Res.*, vol. 51, no. 22, pp. 7656–7662, 2012.

[15] M. Hertzberg, I. A. Zlochower, and K. L. Cashdollar, “V O L a T I L I T Y M O D E L for Coal D U S T Flame P R O P a G a T I O N a N D,” pp. 325–333, 1986.

[16] F. C. John E . Going, Jef Snoeys, “Explosion Protection with Metal Dust Fuels 704 South 10 th St Blue Springs , MO 64015 Prepared for presentation at : American Institute of Chemical Engineers 36 th Annual Loss Prevention Symposium New Orleans , L,” *Am. Inst. Chem. Eng.*, pp. 1–20, 2002.

[17] C. Mohabeer, “Bio-oil production by pyrolysis of biomass coupled with a catalytic de-oxygenation treatment,” *Hal*, p. 207, 2019.

[18] A. V. Bridgwater, "Production of high grade fuels and chemicals from catalytic pyrolysis of biomass," *Catal. Today*, vol. 29, no. 1–4, pp. 285–295, 1996.

[19] A. Dufour, B. Ouartassi, R. Bounaceur, and A. Zoulalian, "Modelling intra-particle phenomena of biomass pyrolysis," *Chem. Eng. Res. Des.*, vol. 89, no. 10, pp. 2136–2146, 2011.

[20] O. Onay and O. M. Kockar, "Slow, fast and flash pyrolysis of rapeseed," *Renew. Energy*, vol. 28, no. 15, pp. 2417–2433, 2003.

[21] P. A. Horne and P. T. Williams, "Influence of temperature on the products from the flash pyrolysis of biomass," *Fuel*, vol. 75, no. 9, pp. 1051–1059, 1996.

[22] A. V. Bridgwater, "Principles and practice of biomass fast pyrolysis processes for liquids," *J. Anal. Appl. Pyrolysis*, vol. 51, no. 1, pp. 3–22, 1999.

[23] L. Li, J. S. Rowbotham, H. Christopher Greenwell, and P. W. Dyer, *An Introduction to Pyrolysis and Catalytic Pyrolysis: Versatile Techniques for Biomass Conversion*. 2013.

[24] A. V. Bridgwater, "Review of fast pyrolysis of biomass and product upgrading," *Biomass and Bioenergy*, vol. 38, pp. 68–94, 2012.

[25] M. Keiluweit, P. S. Nico, M. G. Johnson, and M. KLEBER, "Dynamic Molecular Structure of Plant Biomass-derived Black Carbon(Biochar)- Supporting Information -," *Environ. Sci. Technol.*, vol. 44, no. 4, pp. 1247–1253, 2010.

[26] R. Azargohar, S. Nanda, J. A. Kozinski, A. K. Dalai, and R. Sutarto, "Effects of temperature on the physicochemical characteristics of fast pyrolysis bio-chars derived from Canadian waste biomass," *Fuel*, vol. 125, pp. 90–100, 2014.

[27] S. Omar, S. Alsamaq, Y. Yang, and J. Wang, "Production of renewable fuels by blending bio-oil with alcohols and upgrading under supercritical conditions," *Front. Chem. Sci. Eng.*, vol. 13, no. 4, pp. 702–717, 2019.

[28] W. L. H. Hallett and N. A. Clark, "A model for the evaporation of biomass pyrolysis oil droplets," *Fuel*, vol. 85, no. 4, pp. 532–544, 2006.

[29] D. A. Bulushev and J. R. H. Ross, "Catalysis for conversion of biomass to fuels via pyrolysis and gasification: A review," *Catal. Today*, vol. 171, no. 1, pp. 1–13, 2011.

[30] J. G. Brammer, M. Lauer, and A. V. Bridgwater, "Opportunities for biomass-derived 'bio-oil' in European heat and power markets," *Energy Policy*, vol. 34, no. 17, pp. 2871–2880, 2006.

[31] H. B. Goyal, D. Seal, and R. C. Saxena, "Bio-fuels from thermochemical conversion of renewable resources: A review," *Renew. Sustain. Energy Rev.*, vol. 12, no. 2, pp. 504–517, 2008.

[32] A. V. Bridgwater, S. Czernik, and J. Piskorz, "An Overview of Fast Pyrolysis," *Prog. Thermochem. Biomass Convers.*, no. 1, pp. 977–997, 2008.

[33] Q. Lu, X. C. Yang, C. Q. Dong, Z. F. Zhang, X. M. Zhang, and X. F. Zhu, "Influence of pyrolysis temperature and time on the cellulose fast pyrolysis products: Analytical Py-GC/MS study," *J. Anal. Appl. Pyrolysis*, vol. 92, no. 2, pp. 430–438, 2011.

[34] Y. Le Brech, L. Jia, S. Cissé, G. Mauviel, N. Brosse, and A. Dufour, "Mechanisms of biomass pyrolysis studied by combining a fixed bed reactor with advanced gas analysis," *J. Anal. Appl. Pyrolysis*, vol. 117, pp. 334–346, 2016.

[35] J. Sarkar and S. Bhattacharyya, "Application of graphene and graphene-based materials in

clean energy-related devices Minghui," *Arch. Thermodyn.*, vol. 33, no. 4, pp. 23–40, 2012.

[36] P. Fu, W. Yi, X. Bai, Z. Li, S. Hu, and J. Xiang, "Effect of temperature on gas composition and char structural features of pyrolyzed agricultural residues," *Bioresour. Technol.*, vol. 102, no. 17, pp. 8211–8219, 2011.

[37] L. Wei *et al.*, "Characteristics of fast pyrolysis of biomass in a free fall reactor," *Fuel Process. Technol.*, vol. 87, no. 10, pp. 863–871, 2006.

[38] D. Czajczyńska, R. Krzyżyńska, H. Jouhara, and N. Spencer, "Use of pyrolytic gas from waste tire as a fuel: A review," *Energy*, vol. 134, pp. 1121–1131, 2017.

[39] A. V. Bridgwater, "The production of biofuels and renewable chemicals by fast pyrolysis of biomass," *Int. J. Glob. Energy Issues*, vol. 27, no. 2, pp. 160–203, 2007.

[40] Y. Yang *et al.*, "Characterisation of waste derived intermediate pyrolysis oils for use as diesel engine fuels," *Fuel*, vol. 103, pp. 247–257, 2013.

[41] A. V. Bridgwater, "Renewable fuels and chemicals by thermal processing of biomass," *Chem. Eng. J.*, vol. 91, no. 2–3, pp. 87–102, 2003.

[42] D. Mohan, C. U. Pittman, and S. Philip, "Pyrolysis of Wood/Biomass for Bio-oil: A Critical Review Dinesh," *Prog. Energy Combust. Sci.*, vol. 62, no. 4, pp. 848–889, 2017.

[43] H. F. Gerçel, "Production and characterization of pyrolysis liquids from sunflower-pressed bagasse," *Bioresour. Technol.*, vol. 85, no. 2, pp. 113–117, 2002.

[44] R. Zanzi, K. Sjöström, and E. Björnbom, "Rapid high-temperature pyrolysis of biomass in a free-fall reactor," *Fuel*, vol. 75, no. 5, pp. 545–550, 1996.

[45] R. Zanzi, K. Sjöström, and E. Björnbom, "Rapid pyrolysis of agricultural residues at high temperature," *Biomass and Bioenergy*, vol. 23, no. 5, pp. 357–366, 2002.

[46] J. M. Commandré, H. Lahmidi, S. Salvador, and N. Dupassieux, "Pyrolysis of wood at high temperature: The influence of experimental parameters on gaseous products," *Fuel Process. Technol.*, vol. 92, no. 5, pp. 837–844, 2011.

[47] S. Li, S. Xu, S. Liu, C. Yang, and Q. Lu, "Fast pyrolysis of biomass in free-fall reactor for hydrogen-rich gas," *Fuel Process. Technol.*, vol. 85, no. 8–10, pp. 1201–1211, 2004.

[48] A. E. Pütün, N. Özbay, E. P. Önal, and E. Pütün, "Fixed-bed pyrolysis of cotton stalk for liquid and solid products," *Fuel Process. Technol.*, vol. 86, no. 11, pp. 1207–1219, 2005.

[49] A. A. Boateng, D. E. Daugaard, N. M. Goldberg, and K. B. Hicks, "Bench-scale fluidized-bed pyrolysis of switchgrass for bio-oil production," *Ind. Eng. Chem. Res.*, vol. 46, no. 7, pp. 1891–1897, 2007.

[50] T. Hatsuda, Y. Yamada, J. Osada, T. Kobayasi, Y. Aoki, and T. Kato, "Measured results of urban satellite-diversity (Sat. D) and space-diversity (SD) characteristics for mobile broadcast geostationary satellite system," *IEEE Antennas Propag. Soc. AP-S Int. Symp.*, vol. 3, no. 15, pp. 117–120, 2001.

[51] A. Chaala, T. Ba, M. Garcia-Perez, and C. Roy, "Colloidal properties of bio-oils obtained by vacuum pyrolysis of softwood bark: Aging and thermal stability," *Energy and Fuels*, vol. 18, no. 5, pp. 1535–1542, 2004.

[52] Z. Du *et al.*, "Microwave-assisted pyrolysis of microalgae for biofuel production," *Bioresour. Technol.*, vol. 102, no. 7, pp. 4890–4896, 2011.

[53] J. A. Garcia-Nunez *et al.*, *Historical Developments of Pyrolysis Reactors: A Review*, vol. 31,

no. 6. 2017.

[54] L. Jia, A. Dufour, Y. Le Brech, O. Authier, and G. Mauviel, "On-line analysis of primary tars from biomass pyrolysis by single photoionization mass spectrometry: Experiments and detailed modelling," *Chem. Eng. J.*, vol. 313, pp. 270–282, 2017.

[55] D. Meier and O. Faix, "State of the art of applied fast pyrolysis of lignocellulosic materials - A review," *Bioresour. Technol.*, vol. 68, no. 1, pp. 71–77, 1999.

[56] J. Harmsen and M. Verkerk, "13 Rotating cone reactor biomass pyrolysis process," *Process Intensif.*, pp. 142–151, 2020.

[57] M. Arabiourrutia, G. Elordi, M. Olazar, and J. Bilbao, "Pyrolysis of Polyolefins in a Conical Spouted Bed Reactor: A Way to Obtain Valuable Products," *Pyrolysis*, vol. 2014, 2017.

[58] A. Demirbas, "Heavy metal adsorption onto agro-based waste materials: A review," *J. Hazard. Mater.*, vol. 157, no. 2–3, pp. 220–229, 2008.

[59] B. A. B. Ii and A. J. Manis, "6 10 5)," no. 2012, pp. 5–12, 2009.

[60] W. P. (Georgia I. of T. Ryszytiwskyj, "MINIMUM IGNITION TEMPERATURES OF PYROLYSATE-AIR MIXTURES AS A FUNCTION OF PYROLYSATE CONCENTRATION," Georgia Institute of Technology, 1976.

[61] M. M. Tang and R. Bacon, "Carbonization of cellulose fibers-I. Low temperature pyrolysis," *Carbon N. Y.*, vol. 2, no. 3, pp. 211–220, 1964.

[62] F. Shafizadeh, "Introduction to pyrolysis of biomass," *J. Anal. Appl. Pyrolysis*, vol. 3, no. 4, pp. 283–305, 1982.

[63] O. Boutin, M. Ferrer, and J. Le, "Radiant flash pyrolysis of cellulose — Evidence for the formation of short life time intermediate liquid species," vol. 47, pp. 13–31, 1998.

[64] F. F. Y. L. Shafizadeh, "Pyrolysis Of cellulose," vol. 29, pp. 113–122, 1973.

[65] D. K. Shen and S. Gu, "Bioresource Technology The mechanism for thermal decomposition of cellulose and its main products," *Bioresour. Technol.*, vol. 100, no. 24, pp. 6496–6504, 2009.

[66] P. Mischnick and D. Momcilovic, *Chemical Structure Analysis of Starch and Cellulose Derivatives*, vol. 64, no. 10. Elsevier Inc., 2010.

[67] Q. Li *et al.*, "Effect of pulsed electric field on structural properties and digestibility of starches with different crystalline type in solid state," *Carbohydr. Polym.*, vol. 207, no. October 2018, pp. 362–370, 2019.

[68] P. Zong *et al.*, "Pyrolysis behavior and product distributions of biomass six group components: Starch, cellulose, hemicellulose, lignin, protein and oil," *Energy Convers. Manag.*, vol. 216, no. November 2019, p. 112777, 2020.

[69] M. Pigłowska, B. Kurc, Ł. Rymaniak, P. Lijewski, and P. Fuć, "Kinetics and thermodynamics of thermal degradation of different starches and estimation the OH group and H2O content on the surface by TG/DTG-DTA," *Polymers (Basel).*, vol. 12, no. 2, 2020.

[70] S. Wang, G. Dai, H. Yang, and Z. Luo, "Lignocellulosic biomass pyrolysis mechanism: A state-of-the-art review," *Prog. Energy Combust. Sci.*, vol. 62, pp. 33–86, 2017.

[71] P. Li, J. Estrada, F. Zhang, S. K. Waghmare, and B. Mir, "Isolation, characterization, and nuclear reprogramming of cell lines derived from porcine adult liver and fat," *Cell. Reprogram.*, vol. 12, no. 5, pp. 599–607, 2010.

[72] Z. Yang *et al.*, "Preparation and formation mechanism of levoglucosan from starch using a tubular furnace pyrolysis reactor," *J. Anal. Appl. Pyrolysis*, vol. 102, pp. 83–88, 2013.

[73] M. Balat, "Mechanisms of thermochemical biomass conversion processes. Part 1: Reactions of pyrolysis," *Energy Sources, Part A Recover. Util. Environ. Eff.*, vol. 30, no. 7, pp. 620–635, 2008.

[74] S. Yaman, "Pyrolysis of biomass to produce fuels and chemical feedstocks," *Energy Convers. Manag.*, vol. 45, no. 5, pp. 651–671, 2004.

[75] O. BEAUMONT, "Flash pyrolysis products from beech wood," *Wood fiber Sci.*, vol. 17, no. 2, pp. 228–239, 1985.

[76] K. C. Sembiring, N. Rinaldi, and S. P. Simanungkalit, "Bio-oil from Fast Pyrolysis of Empty Fruit Bunch at Various Temperature," *Energy Procedia*, vol. 65, pp. 162–169, 2015.

[77] J. Yu, N. Paterson, J. Blamey, and M. Millan, "Cellulose, xylan and lignin interactions during pyrolysis of lignocellulosic biomass," *Fuel*, vol. 191, pp. 140–149, 2017.

[78] J. Shigeto, Y. Ueda, S. Sasaki, K. Fujita, and Y. Tsutsumi, "Enzymatic activities for lignin monomer intermediates highlight the biosynthetic pathway of syringyl monomers in Robinia pseudoacacia," *J. Plant Res.*, vol. 130, no. 1, pp. 203–210, 2017.

[79] D. Kai, M. J. Tan, P. L. Chee, Y. K. Chua, Y. L. Yap, and X. J. Loh, "Towards lignin-based functional materials in a sustainable world," *Green Chem.*, vol. 18, no. 5, pp. 1175–1200, 2016.

[80] W. J. Liu, H. Jiang, and H. Q. Yu, "Thermochemical conversion of lignin to functional materials: a review and future directions," *Green Chem.*, vol. 17, no. 11, pp. 4888–4907, 2015.

[81] J. Zakzeski, P. C. A. Bruijnincx, A. L. Jongerius, and B. M. Weckhuysen, "The catalytic valorization of lignin for the production of renewable chemicals," *Chem. Rev.*, vol. 110, no. 6, pp. 3552–3599, 2010.

[82] Y. Pu, S. Cao, and A. J. Ragauskas, "Application of quantitative 31P NMR in biomass lignin and biofuel precursors characterization," *Energy Environ. Sci.*, vol. 4, no. 9, pp. 3154–3166, 2011.

[83] P. R. Patwardhan, R. C. Brown, and B. H. Shanks, "Understanding the fast pyrolysis of lignin," *ChemSusChem*, vol. 4, no. 11, pp. 1629–1636, 2011.

[84] W. Jin, K. Singh, and J. Zondlo, "Pyrolysis kinetics of physical components of wood and wood-polymers using isoconversion method," *Agric.*, vol. 3, no. 1, pp. 12–32, 2013.

[85] B. L. C. Pereira, A. de Angélica de C.O. Carneiro, A. M. M. L. Carvalho, J. L. Colodette, A. C. Oliveira, and M. P. F. Fontes, "Influence of Chemical Composition of Eucalyptus Wood on Gravimetric Yield and Charcoal Properties," *BioResources*, vol. 8, no. 2, pp. 4574–4592, 2013.

[86] I. Y. Mohammed, Y. A. Abakr, F. K. Kazi, S. Yusup, I. Alshareef, and S. A. Chin, "Comprehensive characterization of Napier grass as a feedstock for thermochemical conversion," *Energies*, vol. 8, no. 5, pp. 3403–3417, 2015.

[87] X. J. Guo, S. R. Wang, K. G. Wang, Q. Liu, and Z. Y. Luo, "Influence of the extractives on mechanism of biomass pyrolysis," *Ranliao Huaxue Xuebao/Journal Fuel Chem. Technol.*, vol. 38, no. 1, pp. 42–46, 2010.

[88] M. Melzer, J. Blin, A. Bensakhria, J. Valette, and F. Broust, "Pyrolysis of extractive rich agroindustrial residues," *J. Anal. Appl. Pyrolysis*, vol. 104, pp. 448–460, 2013.

[89] S. V. Vassilev, D. Baxter, L. K. Andersen, and C. G. Vassileva, "An overview of the chemical composition of biomass," *Fuel*, vol. 89, no. 5, pp. 913–933, 2010.

[90] M. J. F. Llorente and J. E. C. García, "Concentration of elements in woody and herbaceous biomass as a function of the dry ashing temperature," *Fuel*, vol. 85, no. 9, pp. 1273–1279, 2006.

[91] C. Mohabeer, L. Abdelouahed, S. Marcotte, and B. Taouk, "Comparative analysis of pyrolytic liquid products of beech wood, flax shives and woody biomass components," *J. Anal. Appl. Pyrolysis*, vol. 127, no. January, pp. 269–277, 2017.

[92] C. H. Pang, S. Gaddipatti, G. Tucker, E. Lester, and T. Wu, "Relationship between thermal behaviour of lignocellulosic components and properties of biomass," *Bioresour. Technol.*, vol. 172, pp. 312–320, 2014.

[93] A. George, T. J. Morgan, and R. Kandiyoti, "Pyrolytic reactions of lignin within naturally occurring plant matrices: Challenges in biomass pyrolysis modeling due to synergistic effects," *Energy and Fuels*, vol. 28, no. 11, pp. 6918–6927, 2014.

[94] A. Demirbas, "The influence of temperature on the yields of compounds existing in bio-oils obtained from biomass samples via pyrolysis," *Fuel Process. Technol.*, vol. 88, no. 6, pp. 591–597, 2007.

[95] C. Fushimi, S. Katayama, and A. Tsutsumi, "Elucidation of interaction among cellulose, lignin and xylan during tar and gas evolution in steam gasification," *J. Anal. Appl. Pyrolysis*, vol. 86, no. 1, pp. 82–89, 2009.

[96] T. Hosoya, H. Kawamoto, and S. Saka, "Pyrolysis behaviors of wood and its constituent polymers at gasification temperature," *J. Anal. Appl. Pyrolysis*, vol. 78, no. 2, pp. 328–336, 2007.

[97] C. E. Greenhalf, D. J. Nowakowski, A. B. Harms, J. O. Titiloye, and A. V. Bridgwater, "A comparative study of straw, perennial grasses and hardwoods in terms of fast pyrolysis products," *Fuel*, vol. 108, no. February, pp. 216–230, 2013.

[98] Y. Le Brech, L. Jia, S. Cissé, G. Mauviel, N. Brosse, and A. Dufour, "Mechanisms of biomass pyrolysis studied by combining a fixed bed reactor with advanced gas analysis," *J. Anal. Appl. Pyrolysis*, vol. 117, pp. 334–346, 2016.

[99] D. Chen, A. Gao, K. Cen, J. Zhang, X. Cao, and Z. Ma, "Investigation of biomass torrefaction based on three major components: Hemicellulose, cellulose, and lignin," *Energy Convers. Manag.*, vol. 169, pp. 228–237, 2018.

[100] R. K. Eckhoff, "Origin and development of the Godbert-Greenwald furnace for measuring minimum ignition temperatures of dust clouds," *Process Saf. Environ. Prot.*, vol. 129, pp. 17–24, 2019.

[101] "Laboratory Studies of the Inflammability of Coal Dusts: Effects of Fineness ... - Albert Lawrence Godbert, Charles Freeman Jackson, Kenneth Keith Kelley, Ralph Homeward Espach, Strathmore Ridley Barnott Cooke, Thomas Garfield Chapman, William Waugh Adams,." [Online]. Available: https://books.google.fr/books?hl=en&lr=&id=ukENvbScrSwC&oi=fnd&pg=PA1&ots=ppGMmaENjX&sig=rXSU-VMCt8udW9TNZdqi7BTHnaQ&redir_esc=y#v=onepage&q&f=false. [Accessed: 09-Jul-2021].

[102] J. Deng *et al.*, "Minimum ignition temperature of aluminium dust clouds via the Godbert–Greenwald furnace," *Process Saf. Environ. Prot.*, vol. 129, pp. 176–183, 2019.

[103] N. A. Shaarani, “LASER PARTICLE SIZE ANALYSER : APPLICATION FOR MARINE SEDIMENTS,” no. June, 2016.

[104] A. Rawle, M. I. Limited, E. B. Park, and G. Road, “粒度简介,” *Surf. Coatings Int. Part A Coatings J.*, vol. 44, no. 0, pp. 1–8, 2003.

[105] “Hydro SM Small volume wet dispersion for Mastersizer | Malvern Panalytical.” [Online]. Available: https://www.malvernpanalytical.com/en/products/product-range/mastersizer-range/mastersizer-3000e/accessories/hydro-sm/. [Accessed: 02-Jul-2021].

[106] C. Weiler, M. Wolkenhauer, M. Trunk, and P. Langguth, “New model describing the total dispersion of dry powder agglomerates,” *Powder Technol.*, vol. 203, no. 2, pp. 248–253, 2010.

[107] M. Pietraccini, S. Audrey, M. Verdonck, A. Dufour, P.-A. Glaude, and O. Dufaud, “(11c) Dust Explosions: A New Path to Estimate the Explosibility Characteristics of an Organic Powder | AIChE Academy,” *submitted to the Journal of Loss Prevention in the Process Industries, under review*. [Online]. Available: https://www.aiche.org/academy/conferences/aiche-spring-meeting-and-global-congress-on-process-safety/2021/proceeding/paper/11c-dust-explosions-new-path-estimate-explosibility-characteristics-organic-powder. [Accessed: 24-Jul-2021].

[108] “Minimum Ignition Temperature of dust clouds (MIT).” [Online]. Available: https://powderprocess.net/Safety/Dust_Minimum_Ignition_Temperature_MIT.html. [Accessed: 08-Jul-2021].

[109] V. De Schepper, D. Van Dusschoten, P. Copini, S. Jahnke, and K. Steppe, “MRI links stem water content to stem diameter variations in transpiring trees,” *J. Exp. Bot.*, vol. 63, no. 7, pp. 2645–2653, 2012.

[110] S. RF, *Compressed Tablets by Direct Compression Granulation Pharmaceutical Dosage Forms*, vol. 1. 1989.

[111] A. Di Benedetto and P. Russo, “Thermo-kinetic modelling of dust explosions,” *J. Loss Prev. Process Ind.*, vol. 20, no. 4–6, pp. 303–309, 2007.

[112] L. J. R. Nunes, J. C. De Oliveira Matias, and J. P. Da Silva Catalão, “Applications for Torrefied Biomass,” *Torrefaction Biomass Energy Appl.*, pp. 203–214, 2018.

[113] S. Li, J. Lyons-Hart, J. Banyasz, and K. Shafer, “Real-time evolved gas analysis by FTIR method: An experimental study of cellulose pyrolysis,” *Fuel*, vol. 80, no. 12, pp. 1809–1817, 2001.

[114] D. Fabbri, C. Torri, and V. Baravelli, “Effect of zeolites and nanopowder metal oxides on the distribution of chiral anhydrosugars evolved from pyrolysis of cellulose: An analytical study,” *J. Anal. Appl. Pyrolysis*, vol. 80, no. 1, pp. 24–29, 2007.

[115] J. Piskorz, P. Majerski, D. Radlein, A. Vladars-Usas, and D. S. Scott, “Flash pyrolysis of cellulose for production of anhydro-oligomers,” *J. Anal. Appl. Pyrolysis*, vol. 56, no. 2, pp. 145–166, 2000.

[116] S. Sun, H. Tian, Y. Zhao, R. Sun, and H. Zhou, “Experimental and numerical study of biomass flash pyrolysis in an entrained flow reactor,” *Bioresour. Technol.*, vol. 101, no. 10, pp. 3678–3684, 2010.

[117] A. Janès, A. Vignes, O. Dufaud, and D. Carson, “Experimental investigation of the influence of inert solids on ignition sensitivity of organic powders,” *Process Saf. Environ. Prot.*, vol. 92, no. 4, pp. 311–323, 2014.

[118] W. Jaskolkowski, S. Ptak, A. Laskowski, and G. Zakrzewska, “Effects of particle size on minimum ignition temperature of dust layers and dust clouds of selected wood dusts,” *Ann. Warsaw Univ. Life Sci. - SGGW. For. Wood Technol.*, vol. 86, pp. 138–143, 2014.

ANNEXE

Annexe 1: Mass yields of powder segregation in the G—G setup.

Annexe 2: Cellulose and Wheat Starch tar composition and their yields

Annexe 3: Calculations for molar ratios on dry gas compositions.

The link to Annexes 1 – 3 can be accessed from the attached link in this document.

https://drive.google.com/drive/folders/1AEV9mx-09gmBB9SUjfy779374cihjWVQ?usp=sharing

Annexe 4 (a) : Experimental data for cellulose (Avicel PH 101) dust cloud Minimum Ignition Temperature (MIT) determination.

T (°C)	ΔP (mbar)	m (mg)	Observation
440	200	200	Gaseous Product
450	200	200	Gaseous Product
470	200	200	Gaseous Product
490	200	200	Gaseous Product
500	200	200	Gaseous Product
510	200	200	Gaseous Product
520	200	200	Flame present
Parametric Study			
520	100	200	Gaseous Product
520	300	200	Bright flame
520	200	100	Gaseous Product
520	300	100	Dim flame
520	300	300	Brightest Visible flame
520	100	300	No visible flame
Search for Minimum			
510	300	300	Bright Flame
500	300	300	Bright Flame
460	300	300	Dim Visible Flame
Following Test Performed 10 times: no Ignition			
440	300	300	No Ignition
MIT Observed: 460°C MIT standard (-20°C if > 300°C) = 440°C MIT standard (-10°C if < 300°C)			

Annexe 4 (b): Experimental data for wheat starch dust cloud Minimum Ignition Temperature (MIT) determination.

T (°C)	ΔP (mbar)	m (mg)	Observation
300	200	200	No visible flame
330	200	200	Gaseous Product
350	200	200	Gaseous Product
370	200	200	Gaseous Product
400	200	200	Gaseous Product
420	200	200	Gaseous Product
440	200	200	Gaseous Product
460	200	200	Gaseous Product
510	200	200	Visible Flame
Parametric Study			
510	100	200	No flame
510	300	200	Bright flame
510	200	100	Short and Bright Flame
510	300	100	Flame Present
510	300	300	Brightest flame
510	100	300	No flame
Search for Minimum			
490	300	300	Flame Present
470	300	300	Flame Present
460	300	300	Flame Present
450	300	300	Weakest Flame present
Following Test Performed 10 times: no Ignition			
430	300	300	No Ignition
MIT Observed: 450°C			
MIT standard (-20°C if > 300°C) = 430°C			
MIT standard (-10°C if < 300°C)			

Annexe 4 (c): Experimental data for oak dust cloud Minimum Ignition Temperature (MIT) determination.

T (°C)	ΔP (mbar)	m (mg)	Observation

600	200	200	Bright flame
530	200	200	Mild Flame
500	200	200	Weak Flame
Parametric Study			
500	100	200	No flame
500	300	200	Mild Flame with Sparks
500	200	100	Gaseous Product
500	300	100	No flame
500	300	300	Brightest flame
500	100	300	No flame
Search for Minimum			
490	300	300	Gaseous Product with a weak flame
Following Test Performed 10 times: no Ignition			
470	300	300	No Ignition
MIT Observed: 490^{o}C MIT standard (-20^{o}C if > 300^{o}C) = 470^{o}C MIT standard (-10^{o}C if < 300^{o}C)			